

ESD REPRODUCTION COPY

RETURN TO
SCIENTIFIC & TECHNICAL INFORMATION DIVISION
(ESTI), BUILDING 1211

ESD ACCESSION LIST

ESTI Call No. _____
Copy No. 1 of 2 cys
AL 58888

ESD-TR-67-564
FILE COPY

Technical Note

1967-50

Long-Period
Signal Processing Results
For Large Aperture
Seismic Array

J. Capon
R. J. Greenfield
R. T. Lacoss

15 November 1967

Prepared for the Advanced Research Projects Agency
under Electronic Systems Division Contract AF 19(628)-5167 by

Lincoln Laboratory

MASSACHUSETTS INSTITUTE OF TECHNOLOGY

Lexington, Massachusetts



ADD 66 3429

The work reported in this document was performed at Lincoln Laboratory, a center for research operated by Massachusetts Institute of Technology. This research is a part of Project Vela Uniform, which is sponsored by the U.S. Advanced Research Projects Agency of the Department of Defense, it is supported by ARPA under Air Force Contract AF 19(628)-5167 (ARPA Order 512).

This report may be reproduced to satisfy needs of U.S. Government agencies.

This document has been approved for public release and sale; its distribution is unlimited.

MASSACHUSETTS INSTITUTE OF TECHNOLOGY
LINCOLN LABORATORY

LONG-PERIOD SIGNAL PROCESSING RESULTS
FOR LARGE APERTURE SEISMIC ARRAY

J. CAPON

R. J. GREENFIELD

R. T. LACOSS

Group 64

TECHNICAL NOTE 1967-50

15 NOVEMBER 1967

LEXINGTON

MASSACHUSETTS

ABSTRACT

The results of a series of off-line signal processing experiments are presented for long-period data obtained from the Large Aperture Seismic Array (LASA) located in eastern Montana. The signal-to-noise ratio gains obtained with maximum-likelihood processing, as well as other simpler forms of processing, are presented for body-wave as well as surface-wave phases. A discussion of the frequency-wavenumber characteristics of the noise which led to these results is also given. On the basis of these experiments several recommendations are made concerning optimum long-period array configurations and on-line or off-line processing methods.

The usefulness of maximum-likelihood processing in suppressing an interfering teleseism is demonstrated. An experiment is given in which maximum-likelihood processing achieved about 20 db suppression of an interfering teleseism, while simpler forms of processing such as beamforming obtained about 11 db.

The matched filtering of surface waves using chirp waveforms is also discussed. The most useful discriminant for distinguishing between natural seismic events and underground nuclear explosions, using both the long-period and short-period data, was found to be that based on the relationship between the surface-wave and body-wave magnitudes. Measurements of this discriminant made on events from four tectonic regions of the earth are presented. It is shown that 60, 100 percent detectability of surface waves for natural seismic events from the Central Asian-Kurile Islands-Kamchatka region occurs at about LASA body-wave magnitudes 4.5, 4.9, respectively.

Accepted for the Air Force
Franklin C. Hudson
Chief, Lincoln Laboratory Office

TABLE OF CONTENTS

ABSTRACT	iii
I. INTRODUCTION	1
II. SIGNAL-TO-NOISE RATIO GAIN FOR VARIOUS FORMS OF ARRAY PROCESSING	5
III. SUPPRESSION OF LONG-PERIOD INTERFERING TELESEISM	17
IV. MATCHED FILTERING OF LONG-PERIOD SURFACE WAVES	19
V. SURFACE-WAVE <u>VS</u> BODY-WAVE MAGNITUDE DISCRIMINATION RESULTS	24
VI. CONCLUSIONS	35
APPENDIX A. DERIVATION OF SIGNAL-TO-NOISE RATIO GAIN OF MATCHED FILTERS USING CHIRP WAVEFORMS	39
APPENDIX B. COMPUTATION OF PROBABILITY OF NOISE EXCEEDING A SPECIFIED THRESHOLD	45
REFERENCES	47

I. INTRODUCTION

A series of off-line signal processing experiments have been performed using the long-period (LP) data from the Large Aperture Seismic Array (LASA).¹ The LASA consists of 21 subarrays of 25 short-period vertical seismometers as indicated in Fig. 1. An extensive discussion of the short-period (SP) signal processing results for LASA has been given previously.² At the center of each subarray there is a three-component set of LP seismometers oriented in the vertical (Z), north-south (NS), and east-west (EW) directions. The LP array at LASA went into operation about November 1966. The manner in which the various LP phases propagate in the earth is shown in Fig. 2.

One of the major objectives of the LP signal processing experiments was to determine the signal-to-noise ratio (SNR) gain obtained with various forms of array processing. The three array processing schemes employed have been described in detail previously.³ The simplest is delay-and-sum, which will be referred to as DS processing, or beamforming, in which only a steering delay which aligns the signals is applied to each seismometer output before summation. This procedure steers the main lobe of the array beam pattern, but makes no attempt to steer sidelobes and nulls for further noise minimization. The next method, in order of complexity, is weighted-delay-and-sum, or WDS, and attempts to steer sidelobes and nulls of the array beam pattern by applying an amplitude coefficient to each element in addition to the steering delay.

The most complicated of the three methods, filter-and-sum, or FS, establishes a delay and amplitude weight for each element at each resolvably different frequency by applying a filter to each element and then summing filter outputs.

The delays, weights and filter-and-sum operations were synthesized on a digital computer, namely the IBM 360/67. The amplitude weighting coefficients for WDS and the filter functions for FS were designed from noise data observed over a time period called the fitting interval which usually immediately precedes the arrival of the event. The particular approach used in the design of these parameters is the maximum-likelihood method. The maximum-likelihood method is based on the assumption that the event propagates across the array as a plane wave with no significant dispersion so that the signal in each sensor is the same except possibly for a time delay. Subject to this assumption, the maximum-likelihood array processing methods, such as WDS and FS, possess the feature that they produce an output trace in which no distortion is imposed on the signal seismogram waveform.

There is a finite number of coefficients, or degrees of freedom, to be determined in the synthesis procedures for WDS and FS. For WDS this is equal to the number of seismometers, NS, and for FS it is equal to the number of seismometers times the number of filter points, NFP, that specify each filter function. The synthesis procedure will deploy these available degrees of freedom to minimize whatever noise is present in the set of traces observed in the fitting interval. Thus, it is important whether the traces have been prefiltered. Prefiltering operations are quite

effective in suppressing noise whose spectral components lie outside the LP signal frequency band of .025 to .05 Hz, or the 20 to 40 sec period range.

Three forms of prefilters were used in our studies: 1) no prefilter, 2) a bandpass convolutional filter whose impulse response is 400 seconds long, and 3) a matched, or chirp, filter, which is designed to maximize the signal-to-noise ratio for LP dispersed surface waves. The frequency response characteristic of the bandpass filter used is shown in Fig. 3a and that for the chirp filter in Fig. 3b. The results of Fig. 3b pertain to epicentral distances of 85° for events from the Eastern Kazakh region, but tends to be typical of results for epicentral distances between 50 and 90 degrees.

It should be mentioned that in actually performing off-line processing it is customary for the analyst to examine the traces to be combined and delete those occasional ones which have an event which is smaller by about 6 db or more than the average of those traces which are to be processed. If the event is not visible, then traces with anomalously low noise levels are deleted. If this is done, the amount of signal amplitude loss in the final processed output trace, for those signal frequency groups which are designed to be passed by the processing, is seldom more than 1.5 to 2.0 db. This factor will therefore be ignored in most of what follows.

Another objective was to determine the effectiveness of array processing methods in the suppression of interfering LP surface waves. The time duration of these surface waves is usually about 10 to 20 minutes, so that it is quite likely that an

event may generate surface waves which interfere with those of a desired event. This is an area in which FS processing has been found to be much more useful than simpler forms of processing such as DS.

It was also desired to determine how much SNR gain can be obtained by matched filtering of the dispersive surface waves. The matched filtering was performed with simple chirp filters which would be optimum if the group delay were a linear function of frequency and if the spectrum of the surface-wave signal, and that of the noise, were uniform with frequency over the seismometer pass band. These filters were found to provide satisfactory performance and yielded an average SNR gain of about 8 db, for events with epicenters about 80° from LASA.

The final objective of the LP signal processing experiments was to use the LP data, in conjunction with the SP data, to determine discriminants which are useful for distinguishing between natural seismic events and underground nuclear explosions. The most useful discriminant was found to be that which is based on the relationship between the surface-wave and body-wave magnitudes. An extensive study of this discriminant was made and the results will be presented subsequently.

II. SIGNAL-TO-NOISE RATIO GAIN FOR VARIOUS FORMS OF ARRAY PROCESSING

The data were obtained from recordings of the long-period three-component seismometers at LASA. There are 21 sets of three-component instruments, each set is located at the center of a subarray, and thus there is a total of 63 LP seismometers. The sampling rate of the data on the LASA tape is 5 Hz, however, the data were decimated by a factor of 5 so that the sampling rate in all of the experiments performed was 1 Hz. The nominal system transfer function for the LP seismometers is shown in Fig. 4. The important parameters of the LP instruments are given in Table I. The data are quantized by using 14 bits, one bit for sign.

The basic assumption in the filter synthesis procedure for FS and WDS is that the event propagates across the array as a plane wave with no significant differential dispersion so that the signal is the same in each sensor except possibly for a time delay. Theoretical calculations made with meaningful phase velocity curves have shown that the dependence of phase velocity on frequency will not lead to the degradation of the output of a properly steered DS beam. It is also assumed that the epicenter of the event has been located with reasonable accuracy by means of the short-period P-wave. Thus, the time delays required for the LP P- and S-phase processing can be obtained by looking up the appropriate phase velocity in standard seismological tables and using this in conjunction with the azimuth of the event. It was found experimentally that the phase velocity of the 25-sec period group of the LP Rayleigh surface-wave signal was 3.7 km/sec and this velocity, in conjunction with the azimuth of the event, was used to compute the time delays required for the Rayleigh wave processing. It was found that this procedure was

TABLE I

INSTRUMENT NATURAL PERIOD	20 SECONDS
INSTRUMENT DAMPING	0.64 OF CRITICAL DAMPING
AMPLIFIER GAIN	45,000 (UNFILTERED)
FILTER CENTER FREQUENCY	0.04 Hz
SLOPE OF ATTENUATION	80 db/DECADE

BASIC CONSTANTS OF THE LONG-PERIOD SYSTEM

satisfactory for passing, with very little attenuation, the other period groups of the Rayleigh wave. The noise characteristics are estimated in the fitting interval and an FS filter is synthesized on the basis of this measurement. The filter synthesis is performed by evaluating the NFP weighting coefficients of a convolutional filter for each of the NS sensors used.

The important variable parameters used in the design of the filters for FS and the amplitude weights for WDS, given a certain NS and a fixed array geometry, are the length of the fitting interval, NFP and NIM, where every NIMth data point is used in the fitting interval to estimate noise characteristics. It was found that the most reasonable choice of NIM was 2. NIM did not need to be less than 2 because it was found that there was very little noise energy above 0.5 Hz, and a larger value for NIM tended to lead to aliasing due to frequency foldover. The length of the fitting interval was set at one hour as a compromise between stability of the estimates of noise characteristics and computation time. A value of NFP = 21, corresponding to a filter length of 40 seconds, was found to be adequate. All filters designed for FS processing were two-sided, and were designed by means of the frequency-domain synthesis procedure.³ The computer running time for this program on the IBM 360/67 was typically about 10 minutes, consisting of 3.5 minutes to measure the noise properties of a one-hour noise sample, 0.5 minutes to synthesize the filter and 6 minutes to apply the filter. The SNR gain obtained in the fitting interval was approximately the same as that outside of the fitting interval for a period of about two hours after the

end of the fitting interval. However, the filters must be designed anew for data which are situated in time at more than two hours from the fitting interval.

The array processing results for the LP P-, S- and R-phases will now be given. The LP SNR gains are presented in Table II. The details of the spectra for the Z, NS, EW components are shown in Fig. 5. It should be noted that the Z-component tends to have less noise power than the NS, EW components. This was found to be generally true in processing the data on the three LP components, i. e. , the Z-component tends to be less noisy than the NS and EW components.

The SNR gain for FS, WDS, DS vs frequency is given in Figs. 6, 7, and 8 for a S-wave velocity steering for an event from the Kurile Islands region. The corresponding results for P-wave velocities tend to be similar to those presented in Figs. 6, 7, and 8.

An important objective in the experiments using the LP data was to determine discriminants, which in conjunction with the SP data, would be useful for discriminating between natural seismic events and underground nuclear explosions. As mentioned previously, the most useful discriminant was found to be that which is based on the relationship between the surface-wave and body-wave magnitudes. Thus, the processing of the LP Rayleigh surface waves was extremely important and an extensive investigation of various methods for processing these surface waves was made. It was found that the NS and EW components tended to have, on the average, a noise level which was 10 db higher than that on the Z-component. Thus, the NS, EW components

TABLE II

LONG-PERIOD SIGNAL-TO-NOISE RATIO GAINS (db)

NS = 21, $10 \log NS = 13 \text{ db}$

<u>PHASE</u>	<u>COMPONENT</u>	<u>TYPE OF PROCESSING</u>		
		<u>DS</u>	<u>WDS</u>	<u>FS</u>
P	Z	8-11	12-14	13-16
P	EW	8-13	11-14	12-16
P	NS	7-13	11-14	13-15
S	Z	8-11	12-14	13-16
S	EW	8-13	11-14	12-16
S	NS	7-13	11-14	13-15
R	Z	6-11	12-14	13-16
R	EW	10-12	11-14	12-16
R	NS	9-11	11-14	13-16

NO PREFILTERING

SNR GAINS RELATIVE TO AVERAGE UNFILTERED TRACE

RAYLEIGH WAVE STEERINGS AWAY FROM DIRECTION OF NOISE SOURCE.

were not useful for applying the surface-wave discriminant at low signal-to-noise ratios. It should be mentioned, however, that there were rare occasions when the NS, EW components were not too noisy and provided additional SNR gain in the processing of surface waves. However, even on these rare occasions the NS, EW components provided only 2-3 db more SNR gain than could be obtained with the array of Z components. For this reason, only the Z components will be considered in the ensuing discussion.

As mentioned previously, three forms of prefiltering were used in the processing of the Rayleigh surface waves: 1) no prefilter, 2) a bandpass (BP) convolutional filter whose impulse response is 400 seconds long and whose frequency response characteristic is shown in Fig. 3a, and 3) a matched, or chirp, filter (MF) a typical frequency response for which is shown in Fig. 3b. For DS processing it does not make any difference as to the order in which the processing is performed. For example, BP filtering followed by DS followed by MF filtering, denoted by BP - DS - MF, is equivalent to DS - BP - MF, or for that matter to any one of the other five possible permutations obtained with these three forms of processing. However, the corresponding statement for FS and WDS is not true. If we are interested in the SNR gain in the 20 to 40 second period range, then BP - FS is superior to FS - BP. The reason for this is that the FS processing has a limited number of degrees of freedom with which it can suppress the noise, and these degrees of freedom can be used more effectively if the noise power is concentrated in the signal frequency band. That is, there is no wasting of degrees of freedom for FS on those frequency components of the

noise that lie outside the signal frequency band. Thus, for FS processing it is important to specify the order in which the processing is performed.

The average SNR gains obtained for various forms of processing of Rayleigh surface waves is shown in Table III. For simplicity, only the results for DS and FS are presented. These results were obtained for $NS = 17$ by omitting the B-ring at LASA, since it was found that the inclusion of the B-ring tended to lower the SNR gain of DS due to the highly coherent noise which is introduced by its closely spaced seismometers. It is well to recall that the diameter of the B-ring at LASA is only 20 km. The spectra for a raw, BP and MF filtered LPZ trace is shown in Fig. 9. The SNR gain vs frequency is given in Fig. 10a-c for no prefiltering and for BP, MF prefiltering, respectively, for a noise sample preceding the arrival of Eastern Kazakh event # 2. The traces obtained by various forms of processing for this same Eastern Kazakh event are shown in Fig. 11. We see from these results that there is a small advantage of about 3 db, of the complicated BP - FS - MF, or MF - FS processing schemes over the much simpler DS - MF processing.

It should be stressed once again that the preceding results were obtained for Rayleigh wave steerings away from the direction of the noise source. It has been found from frequency-wavenumber data that much of the noise energy lies in the 16 - 20 second period range and that this energy is highly concentrated at a wavenumber which would correspond to a phase velocity of about 3.5 km/sec. This indicates that the noise is propagating in a surface-wave mode and thus has characteristics very similar

TABLE III

LONG-PERIOD SIGNAL-TO-NOISE RATIO GAINS FOR VARIOUS FORMS OF PROCESSING
OF RAYLEIGH WAVES

TYPE OF PROCESSING			AVERAGE SNR GAIN (db)			TOTAL AVERAGE SNR GAIN (db)
ORDER OF OPERATION						
<u>1st</u>	<u>2nd</u>	<u>3rd</u>	<u>1st</u>	<u>2nd</u>	<u>3rd</u>	
DS	MF	---	11	8	---	19
FS	MF	---	11	8	---	19
BP	DS	MF	0	11	8	19
BP	FS	MF	0	14	8	22
MF	FS	---	8	14	---	22

NS = 17, 10 LOG NS = 12 db
B-RING OMITTED

RAYLEIGH WAVE STEERINGS AWAY FROM DIRECTION OF NOISE SOURCE

MF SNR GAIN FOR DISTANCE OF 80°

ALL SNR GAINS PERTAIN TO 20 – 40 SECOND PERIOD SIGNAL BAND. BP and MF ACHIEVE AN ADDITIONAL SNR GAIN OF 3 – 7 db ON NOISE OUTSIDE THIS SIGNAL BAND.

to those of the LP Rayleigh surface-wave signals. Therefore, if the azimuth used in array processing is the same as the azimuth of the noise source, the array processing gain should be quite low due to the similarity between the desired event and the noise. An experiment was performed to measure the gain of DS and FS processing as a function of azimuth using the LPZ sensors in the A, D, and E rings at LASA. The horizontal phase velocity used was 3.7 km/sec, as usual. The results of this experiment are shown in Fig. 12 for a noise sample taken prior to Eastern Kazakh event # 3. As expected, the gain of both DS and FS processing decreases sharply when the azimuth is in the vicinity of 25° , corresponding to the azimuth of the noise source. The frequency-wavenumber structure of this noise sample is shown in Fig. 13 at a frequency of 0.05 Hz. The numbers in the diagram represent the percentage, with respect to the total noise power, of the noise power on the indicated contour. A single plane wave propagating across the array would yield a peak value of 100 percent and the general appearance of the data would be the same as that in Fig. 13. It is clear from this figure that the noise source lies at an azimuth of 25° and has a phase velocity of about 3.3 km/sec. The coherency of this same noise sample vs sensor separation was determined in the same manner as described previously,² and the results are shown in Fig. 14. This figure shows that the coherency of the LP noise is still as high as 0.5 for sensor separations on the order of 100 km.

A number of experiments were performed using data obtained from the LPZ array at LASA for the purpose of determining LP array configurations which are

optimum for Rayleigh surface-wave processing. The SNR gain obtained from MF – FS and MF – DS processing, was measured as a function of aperture and number of sensors. The experiments were performed in several ways. The gain of the entire array was measured using 21 sensors, and then, successively, it was measured as the outside and inside rings of sensors were removed from the array. The SNR gain was also measured for an array of five sensors consisting of, successively, the A – B, A – C, A – D, A – E, A – F rings. In addition, several results using the A – C – D and A – D – E rings were obtained. The steering parameters used were those for an event whose azimuth is equal to 356° and a horizontal phase velocity of 3.7 km/sec. The data are shown in Fig. 15, which depicts the SNR gain of DS and FS processing relative to \sqrt{NS} , the gain which would be obtained for independent noise, namely $10 \log NS$, vs the element density. The abscissa is also labelled in terms of average sensor separation.

These results show that if the gain relative to \sqrt{NS} is to be approximately 0 db, then for DS or FS processing, respectively, element spacing should be about 45 or 15 km, respectively. However, if the gain relative to \sqrt{NS} is allowed to be – 1 db, then for DS processing the sensor spacing should be approximately 30 km. It should be mentioned that some care is required in seismometer placement in order to avoid large sidelobes in the array beamforming gain pattern which could adversely affect array performance. A check of the array beamforming gain pattern is necessary for minimum spacings of about 30 km or more. The use of DS instead of FS processing is desirable since DS processing is much simpler and less expensive. In addition, FS processing is much more susceptible to anomalies, such as weak sensors, than is DS processing. It should also

be noted that for a given element density, FS processing has only a 3 db advantage over DS processing.

An experiment was also performed to determine the mode of propagation of the LP noise. Towards this end, power spectra for all three components of a 12/29/66 noise sample were taken which showed strong peaks at both 15.5 and 7.7 second periods. The frequency-wavenumber structure of the noise for each of the three components at these two periods showed that the noise was highly organized. At the 7.7 sec period the noise propagation velocity was 3.0 km/sec from an azimuth of 290° , while at the 15.5 sec period the velocity was 3.7 km/sec and the azimuth was 298° . This velocity was obtained by noting the location of the peak obtained in the frequency-wavenumber structure measured for all three components. The velocity and azimuth obtained in this manner were approximately the same for all three components.

Delay-and-sum beams for each component were then steered towards the noise sources. The horizontal beam components were then rotated to give horizontal beams radial and transverse to the direction of the noise source. The coherencies and phase angles between the different components were computed, as described previously.² The results of the computation are given in Table IV. The radial and vertical traces are highly coherent, but both have low coherency with respect to the transverse component. The phase angle between the vertical and radial traces are close to 90° , as is expected for Rayleigh waves. These results indicate that the radial and vertical components of the noise propagate in a Rayleigh mode while the transverse component propagates in a Love mode. It should be noted that much of the noise on the EW, NS components propagates in the Love mode.

TABLE IV

PERIOD (secs)	BEAM* POWER			COHERENCY			RELATIVE PHASE (DEGREES)		
	<u>R</u>	<u>T</u>	<u>Z</u>	<u>R-T</u>	<u>R-Z</u>	<u>T-Z</u>	<u>R-T</u>	<u>R-Z</u>	<u>T-Z</u>
7.7	4.1	6.5	1.0	0.25	0.89	0.25	2	85	12
15.5	1.0	2.1	1.0	0.16	0.95	0.17	39	88	19

* NORMALIZED WITH RESPECT TO Z COMPONENT

R = Radial Component

T = Transverse Component

Z = Vertical Component

IDENTIFICATION OF LONG-PERIOD NOISE AS LOVE AND RAYLEIGH WAVES

III. SUPPRESSION OF LONG-PERIOD INTERFERING TELESEISM

One area in which FS processing has been found to be much more useful than DS processing is in the suppression of interfering long-period Rayleigh waves. The time duration of these surface waves is usually about 10 to 20 min., so that it is quite likely that an event may generate surface waves which interfere with those of a desired event. An experiment was performed to determine the effectiveness of DS and FS processing in suppressing the surface waves of an interfering event while passing the surface waves of the desired event. The interfering event was taken as a 21 November 1966 Kurile Islands event,* and the desired event as a 12 November 1966 Argentina event.† A 12 November 1966 Kurile Islands event‡ was used in the fitting interval to design the filters used in the FS processing. The surface waves of the 12 November 1966 Argentina event were hidden in the surface waves of the 21 November 1966 Kurile Islands event by adding the traces, as indicated in Fig. 16. The entire LPZ array at LASA was used except for sites D3 and F4 which gave anomalous traces. The results of the DS processing (shown in Fig. 16) indicate that the Argentina surface waves are not resolvable, since only 11 db of rejection of the interfering surface waves was obtained with this form of processing. However, the Argentina surface waves are visible in the FS processed trace, as this form of processing achieved about 20 db of

* $t_o = 12:19:18$, $\Delta = 64^\circ$, $Az = 312^\circ$, $h(\text{CGS}) = 40 \text{ km}$, $m_b(\text{LASA}) = 6.0$, $m_b(\text{CGS}) = 5.6$.

† $t_o = 12:54:02$, $\Delta = 93^\circ$, $Az = 143^\circ$, $m_b(\text{LASA}) = 5.0$, unreported by CGS.

‡ $t_o = 12:49:58$, $\Delta = 72^\circ$, $Az = 312^\circ$, $h(\text{CGS}) = 33 \text{ km}$, $m_b(\text{LASA}) = 5.0$, $m_b(\text{CGS}) = 5.8$.

suppression of the interfering surface waves. Thus, FS processing has a clear superiority over simpler forms of processing, such as beamforming, for the purpose of rejecting interfering surface waves.

In the preceding section it was found that FS processing had only a small SNR gain advantage over DS processing even though the noise tended to be highly coherent and highly concentrated in frequency-wavenumber space. The results in the present section show, however, that for the purpose of suppressing an interfering teleseism, FS processing has a clear superiority over DS processing. The reason for this appears to be that the interfering event is much more concentrated in frequency-wavenumber space than is the noise. In order to substantiate this the frequency-wavenumber data for the 11/12/66 Kurile Islands event was obtained using the A, C rings at LASA. The results are shown in Fig. 17a. In Fig. 17b are shown the corresponding results for the noise sample taken prior to Eastern Kazakh event # 3. If the event consisted of a plane wave propagating across the array, then the frequency-wavenumber data would show a peak value of 100 percent and the appearance of the plot would be roughly the same as in Figs. 17a and b. That is, the degree with which the noise is organized in frequency-wavenumber space is indicated by the peak magnitude of the data. In Fig. 17a we see that this value is 95 percent while in Fig. 17b it is 80 percent, providing an indication that an array processing method such as FS, which can steer its nulls and sidelobes in frequency-wavenumber space, should do much better than DS processing. It is interesting to note the degree to which the interfering event, or noise, must be organized in order for FS processing to achieve significant gain relative to DS processing.

IV. MATCHED FILTERING OF LONG-PERIOD SURFACE WAVES

In the period range of interest, the group velocity at which Rayleigh waves propagate decreases with frequency. As a consequence of this dispersive mode of propagation, the amplitude of the Rayleigh wave train decreases with distance r from the source, at the rate $(r)^{-1/2}$. In addition to this loss due to dispersion, there are also losses due to geometric spreading of the wave, and from dissipation. Much of the loss in amplitude due to dispersion may be recovered by the use of a filter whose response is matched to the Rayleigh wave train. If the noise can be assumed to be white over the signal band of approximately 0.025 to 0.050 Hz, then the matched filter is optimum in the sense that it provides the largest SNR enhancement for the long-period Rayleigh wave train.

An equivalent manner in which this optimum SNR enhancement can be obtained is to crosscorrelate the received signal with a reference waveform which is a replica of the Rayleigh wave train. As is well known, the impulse response of the matched filter is a time-reversed, time-shifted version of the crosscorrelator reference waveform. It was found that a simple linear frequency-sweep reference waveform

$$R(t) = \begin{cases} \sin \left[2\pi \left(f_0 + \frac{f_1 - f_0}{2L} t \right) t \right], & 0 \leq t \leq L \\ 0 & , \text{ otherwise} \end{cases}$$

gave satisfactory results, where f_0, f_1 are the initial and final frequencies of the dispersed Rayleigh wave train whose time duration is assumed to be L sec. This reference waveform is also known as a chirp waveform.⁴ It is easily seen that the chirp waveform would be a replica of the Rayleigh wave train if the group delay were a linear function of frequency and if the spectrum of the signal, and that of the noise, were uniform with frequency over the seismometer pass band.

In reality, the noise is not white over the signal band. It is well known that in this case the filter which provides the largest SNR enhancement consists of the tandem combination of a prewhitening filter which whitens the noise followed by a filter whose impulse response is matched to the signal after it has been applied to the prewhitening filter, i. e., the prewhitened signal. The actual prewhitening operation need not be done in the frequency domain with a filter but can be accomplished by amplitude-weighting of the chirp waveform, assuming, of course, that the group delay is a linear function of frequency. This latter assumption has been found to be reasonably valid by actually measuring the group delay for a number of events. Thus, the effect of noise which is not white in the signal band can be countered by amplitude weighting of the chirp waveform. However, several experiments with amplitude weighting showed that there was no significant difference in SNR enhancement obtained by the use of the amplitude-weighted over the unweighted chirp waveform. Therefore, the noise can be approximated as white noise and no prewhitening operation is required.

It is shown in Appendix A that the theoretical SNR power improvement for the matched filter, assuming the Rayleigh wave is a chirp waveform perfectly matched to a filter impulse response which is also a chirp waveform, is given by the time-bandwidth product $(f_1 - f_0) L$. It is found typically that $L = 600$ seconds, $f_0 = 0.025$ Hz and $f_1 = 0.050$ Hz, so that the theoretical gain is equal to a factor of 15 corresponding to 12 db. In practice, it is found that the envelope of the Rayleigh wave train is not uniform. It is shown in Appendix A that this causes the SNR improvement provided by a perfectly matched filter to be lower than the time-bandwidth product, and to be given by a suitably defined equivalent time-bandwidth product. This equivalent time-bandwidth product has been measured as typically 6 to 10 db for natural seismic events and about 8 to 10 db for nuclear explosions. In addition, the SNR improvement provided by the matched filtering of Rayleigh waves using chirp waveforms is usually within a fraction of a db of that predicted by the equivalent time-bandwidth product. Therefore, the amount of SNR gain obtained using matched filters based on chirp waveforms is very close to that which can be obtained with any other filter. In this connection, we mention the work of Alexander and Rabenstine⁵ who have designed matched filters by actually measuring waveforms for events from given epicentral regions. It is also worthwhile to mention that Aki⁶ has used similar methods for the purpose of studying earthquake mechanism.

Two examples of the application of matched filtering to long-period Rayleigh waves generated by presumed nuclear explosions in the Eastern Kazakh area are shown in

Figs. 18(a) and (b), along with the autocorrelation function of the reference waveform shown for $L = 600$ sec [Fig. 18(c)]. This result is quite typical for L in the range 500 to 800 sec, and is presented to illustrate the waveform which can be expected for a perfectly matched condition. The similarity of the autocorrelation function shown in Fig. 18 with the chirp-filtered trace shows that a relatively good match is obtained. The length of the filter used in the results in Figs. 18(a), and (b), was 720 seconds. The initial and final periods of the chirp waveform were always taken as 40 and 20 seconds, respectively. The group velocity characteristic which is implied by the use of this filter was computed and the result is shown in Fig. 19. This group velocity curve compares quite well with experimentally measured group velocities for Eastern Kazakh events.

As mentioned previously, the initial and final periods of all chirp waveforms used were always taken as 40 and 20 sec, respectively, since this corresponds to the signal frequency band of interest. However, the length of the chirp waveform was varied until a best match, or maximum SNR gain, condition was achieved. An example of this is presented in Fig. 20 (a) and (b). The results of Fig. 20(a) show what occurs when a 600 sec chirp waveform is crosscorrelated with chirp waveforms of lengths varying from 540 – 660 sec. The right-hand edges of the various chirp waveforms are lined up with the left-hand edge of the 600 sec chirp waveform and the crosscorrelation is performed by shifting the various chirp waveforms past the 600 sec chirp waveform. This sequence of results is typical of mismatch results obtained for L in the range 500

to 800 seconds. The corresponding results when actual data are used instead of the 600 sec chirp waveform are presented in Fig. 20(b). The resemblance should be noted between the artificially generated waveforms in Fig. 20(a) and the actual data in Fig. 20(b). In particular, the resemblance should be noted between the perfectly matched condition for $L = 600$ in Fig. 20(a) and the result for $L = 720$ in Fig. 20(b).

V. SURFACE-WAVE VS BODY-WAVE MAGNITUDE DISCRIMINATION RESULTS

A useful discriminant for distinguishing between natural seismic events and underground nuclear explosions is based on the relationship between the surface- and body-wave magnitudes. Theoretical calculations due to Keilis-Borok⁷ have shown that the most efficient excitation of surface waves occurs at wavelengths approximately four times the dimension of the source; that is, the source region acts as a quarter-wavelength antenna. The source dimensions for an underground nuclear explosion are usually much smaller than those of an earthquake of comparable body-wave magnitude. Thus, we would expect the earthquakes to excite the longer periods of surface waves more efficiently than the underground nuclear explosions. This conclusion has been verified experimentally by several previous investigators.^{8,9}

An experiment was performed using LASA data to determine how effective a single LASA is in using this discriminant teleseismically. The body- and surface-wave magnitudes for events from four tectonic regions of the earth have been computed. The weaker events have been subjected to both maximum-likelihood and delay-and-sum processing, which achieve about 14 and 11 db of signal-to-noise ratio enhancement, respectively. In addition, if required, matched filtering can be used to achieve another 6 to 10 db of SNR enhancement.

The body-wave magnitude m_b is based on the amplitude of short-period waves recorded at teleseismic distances and is computed according to the formula given by Gutenberg and Richter¹⁰

$$m_b = \log w/T + Q + S$$

where w is the maximum zero-to-peak ground amplitude (in millimicrons) of the first three to four cycles of the P-wave recorded on vertical-component short-period seismometers, T is the period (in seconds) of the observed short-period cycle, Q is a parameter which depends on epicentral distance and focal depth and is tabulated in Fig. 5 of a paper by Gutenberg and Richter,¹⁰ and S is a ground correction representing average station ground conditions which for convenience is taken to be zero in the case of the LASA.

The surface-wave magnitude M_s is based on the amplitude of Rayleigh waves with periods of about 20 sec and is used as a measure of the excitation of the long-period waves. The surface-wave magnitude is computed as

$$M_s = \log A - \log B + C + D$$

where A is the ground amplitude of Rayleigh waves (in millimicrons) with periods of about 20 sec recorded on vertical-component long-period seismometers, $-\log B$ is a parameter which depends on epicentral distance and is tabulated in Table 4 of a paper by Gutenberg,¹¹ and $C + D$ is a correction for station, depth, and radiation pattern, and is (for convenience) taken to be zero. An empirical relationship between M_s and m_b has been formulated by Gutenberg and Richter,¹⁰

$$M_s = 1.59 m_b - 3.97 \quad .$$

This equation relates the amplitudes of surface waves to those of body waves for earthquakes and was determined from a large body of data for earthquakes of body-wave magnitude greater than 6.0.

If matched filtering is required to detect the surface waves, then its output must be used to compute the surface-wave magnitude. This is done by calibrating the output of the matched filter for events which are visible, before the matched filtering is performed, from the desired epicentral region. A threshold-to-rms noise level of 6 db at the suitable arrival time for surface waves, was required at the output of the matched filter, for reasons described in Appendix B.

The results of the experiment are given in Tables V – VIII and in Figs. 21(a) – (d), which shows the M_s vs m_b for various regions, as well as the Gutenberg-Richter empirical relationship. The point plotted with an arrow beneath it in Fig. 21(a) indicates that for that event the surface waves were not detectable. It is seen from Fig. 21(a) that the results are very encouraging since there is a perfect separation between the earthquake and bomb populations for the Central Asian events.

The body-wave magnitude shown in Figs. 21 (a) – (d) was obtained by averaging over several widely separated sensors at LASA, so that a relatively good determination of body-wave magnitude is obtained, compared with what would be obtained at a single conventional type station. It should be mentioned that the surface-wave magnitude data

TABLE V

EPICENTER AND MAGNITUDE DATA FOR THE CENTRAL ASIAN EVENTS

<u>Date</u>	<u>Region</u>	<u>Origin Time</u>			<u>Latitude (deg. N)</u>	<u>Longitude (deg. E)</u>	<u>Depth (km)</u>	<u>m_b</u>	<u>M_s</u>
		<u>h</u>	<u>m</u>	<u>s</u>					
1966									
Nov. 25	E. Kazakh	20	32	11	49	75	0	4.7	4.5
1967									
Jan. 5	Mongolia	00	15	03	51	111	88	5.8	6.5
Jan. 5	USSR-Mongolia	23	58	31	49	108	+	5.1	4.9
Jan. 18	E. Russia	05	34	44	57	125	11	5.3	6.0
Jan. 20	USSR-Mongolia	01	57	36	50	104	40	5.4	6.1
Jan. 20	USSR-Mongolia	03	28	55	49	108	33	5.0	4.7
Jan. 20	USSR-Mongolia	06	23	26	49	108	33	4.8	4.3
Jan. 22	USSR-Mongolia	12	01	59	49	108	33	5.1	4.6
Feb. 10	Sinkiang	05	50	52	39	87	23	5.3	4.8
Feb. 11	Lake Baikal	09	27	47	53	113	5	5.2	5.0
Feb. 19	Mongolia	20	08	46	46	93	33	4.8	4.4
Feb. 20	Kashmir-Tibet	15	18	39	33	79	24	5.3	5.0
Mar 23	Mongolia	03	19	51	50	101	+	4.5	3.3
Mar 27	N. E. China	08	58	50	43	120	48	5.2	5.6
Apr 2	E. Siberia	05	11	48	63	138	33	4.4	2.8
Apr 22	N. Sinkiang	05	18	56	45	88	+	4.5	3.3
Apr 24	Kashmir-Tibet	08	50	49	32	75	50	5.6	5.0
Apr 25	Mongolia	10	30	43	45	93	33	5.5	4.8
Apr 27	S. Sinkiang	23	14	56	36	87	33	5.5	4.3
Apr 29	Kashmir-Tibet	04	56	33	33	79	33	5.2	4.3
May 8	India-W. Pakistan	18	47	17	29	72	65	5.5	4.6

May 11	N. India	14	50	21	30	76	97	6.2	5.8
May 12	N. India	05	20	32	30	77	33	5.3	4.9
May 14	N. India	09	00	13	28	77	65	5.4	4.9
May 18	India -W.Pakistan	11	30	48	32	75	14	5.3	4.3
May 20	W. Pakistan	08	46	37	29	72	33	5.8	4.7
May 27	Nepal	01	42	08	27	87	80	5.8	5.0
May 27	E. Kazakh	19	06	26	45	80	35	4.9	5.5
May 28	N. India	12	02	27	28	76	45	5.2	4.6
June 2	N. Sinkiang	04	27	36	42	94	33	5.1	3.7
June 7	Mongolia	17	01	08	48	104	33	4.8	4.2
June 24	N. E. China	09	26	08	42	116	33	4.5	3.6
July 28	N. E. China	05	56	13	43	102	30	4.9	4.2
Aug 30	China	04	22	35	36	108	3	5.3	6.4
	*Novaya Zemlya # 1				76	47	0	6.5	4.5
	*E. Kazakh # 2				49	81	0	6.1	3.7
	*E. Kazakh # 3				49	80	0	6.1	3.8
	*E. Kazakh # 4				51	79	0	5.3	2.7
	*E. Kazakh # 5				50	81	0	5.9	2.9
	*E. Kazakh # 6				47	82	0	5.9	3.1
	*E. Kazakh # 7				48	81	0	5.9	3.3
	*E. Kazakh # 8				49	80	0	5.7	3.1
	*E. Kazakh # 9				46	82	0	5.8	less than 2.7

+ Depth not available.

* Presumed nuclear explosion.

TABLE VI
 EPICENTER AND MAGNITUDE DATA FOR
 THE KURILE ISLANDS-KAMCHATKA EVENTS

<u>Date</u>	<u>Region</u>	Origin Time			Latitude (deg. N)	Longitude (deg. E)	Depth (km)	m_b	M_s
		h	m	s					
1966									
Nov 12	Hokkaido	12	49	58	45	146	33	5.0	5.2
Nov 17	Kurile Islands	19	37	37	46	153	33	4.7	3.8
Nov 21	Kurile Islands	12	19	18	46	150	40	6.0	4.5
Nov 21	Kurile Islands	12	30	00	46	152	40	5.9	4.6
Nov 27	Kurile Islands	11	11	20	49	155	40	5.3	3.8
Nov 29	Kurile Islands	08	15	54	48	156	33	4.4	3.2
Nov 29	Kurile Islands	08	19	13	55	154	33	4.4	2.9
Dec 6	Kurile Islands	07	28	35	50	159	27	5.8	3.6
Dec 7	Kurile Islands	04	25	49	46	153	49	4.7	3.0
Dec 7	Kurile Islands	17	17	27	46	153	26	6.0	4.9
Dec 7	Kurile Islands	17	28	30	44	151	33	6.3	5.0
Dec 8	Kommandorsky Is.	15	03	00	55	166	33	4.6	4.5
Dec 17	Kurile Islands	08	12	33	47	149	33	4.2	3.7
Dec 21	Kurile Islands	02	40	58	47	148	33	4.4	3.4
Dec 22	Kurile Islands	12	19	52	52	158	61	4.8	3.4
Dec 22	Kurile Islands	17	37	13	48	147	38	5.0	3.1
Dec 22	Kurile Islands	19	34	21	48	154	77	5.6	3.6
Dec 23	Kurile Islands	23	47	18	53	160	33	4.4	3.1
Dec 23	Kurile Islands	23	58	53	54	162	28	4.9	4.0
Dec 30	Kurile Islands	04	49	48	52	160	33	4.8	3.8
1967									
Jan 18	N. W. of Kuriles	04	20	43	49	152	30	5.4	4.2
Jan 18	Kurile Islands	11	18	04	48	156	$\begin{smallmatrix} + \\ - \end{smallmatrix}$	4.8	4.0

Jan 31	N. W. of Kuriles	17	44	16	46	147	+	4.9	4.2
Feb 13	Kurile Islands	17	05	18	45	148	-	4.9	4.1
Feb 20	E. Sea of Japan	00	35	15	43	140	+	5.0	4.3
Feb 22	Kurile Islands	14	50	30	49	154	-	5.0	4.0
Mar 5	Kurile Islands	10	05	49	47	149	33	5.0	3.3
Mar 6	Hokkaido	09	45	28	45	146	+	4.8	4.0
Mar 12	Kurile Islands	03	46	10	58	155	33	4.2	3.2
Apr 4	Kurile Islands	03	54	12	45	150	39	5.1	4.3
Apr 9	Kurile Islands	21	52	23	46	149	33	4.8	4.0
Apr 13	Sea of Okhotsk	18	41	26	53	154	105	5.7	3.9
Apr 15	Hokkaido	23	35	55	44	142	36	4.9	4.0
Apr 16	Kurile Islands	10	09	52	46	150	60	4.8	4.4
May 7	Off E. C. Kamchatka	08	45	48	55	164	48	5.0	4.0
May 18	Hokkaido	04	06	51	43	144	30	4.8	4.4
May 18	Off C. of Hokkaido	11	22	34	42	147	30	5.3	4.5
May 18	Hokkaido	14	00	53	43	144	30	5.1	4.3
May 19	Sea of Okhotsk	05	26	40	52	150	+	5.0	4.0
May 23	Kurile Islands	01	52	35	45	149	32	5.1	4.4
May 29	Hokkaido	21	01	34	44	144	+	5.2	4.1
June 1	Kamchatka	10	15	52	55	157	57	5.3	4.0
June 1	Kurile Islands	11	03	40	44	147	+	5.5	4.1
June 5	Kamchatka	16	38	35	53	158	57	5.0	4.0
June 7	Kurile Islands	18	16	03	45	151	30	5.6	4.0
June 11	Kurile Islands	11	50	27	50	155	30	5.2	4.2
June 12	Kurile Islands	23	22	20	47	151	42	5.8	5.0
June 13	N. W. of Kuriles	02	42	21	46	149	+	4.9	4.0
June 14	Kurile Islands	08	05	44	48	151	45	5.9	5.2
June 14	Kurile Islands	08	12	42	47	151	48	5.5	4.9
June 28	Kurile Islands	01	09	52	46	149	33	5.5	4.2

+ Depth not available.

TABLE VII

EPICENTER AND MAGNITUDE DATA FOR THE ALEUTIAN ISLANDS EVENTS

<u>Date</u>	<u>Region</u>	<u>Origin Time</u>			<u>Latitude (deg. N)</u>	<u>Longitude (deg. E)</u>	<u>Depth (km)</u>	<u>m_b</u>	<u>M_s</u>
		<u>h</u>	<u>m</u>	<u>s</u>					
1967									
Mar 1	Rat Island	22	16	22	51	179	30	5.4	4.0
Apr 24	Aleutian Islands	16	26	19	49	177	- ⁺	5.0	4.1
Apr 29	Rat Island	03	55	12	51	180	95	6.1	5.0
Apr 29	Rat Island	12	25	21	51	180	42	5.6	4.0
May 4	Near Islands	12	30	10	54	173	48	5.0	3.8
May 7	Andreanof Islands	06	41	02	51	173W	33	5.3	3.9
May 7	Fox Islands	08	11	27	52	169W	45	4.8	3.5
May 7	Rat Island	11	04	00	52	176	- ⁺	4.9	3.8
May 12	Fox Islands	16	58	22	52	169W	45	4.8	3.6
May 12	Andreanof Islands	18	10	39	52	175W	38	4.8	3.5
May 19	Andreanof Islands	16	43	41	51	179W	- ⁺	5.3	3.6
May 20	Fox Islands	01	06	20	53	166W	- ⁺	4.5	2.5
May 20	Fox Islands	08	47	31	53	167W	30	4.5	2.7
May 23	Rat Island	01	19	27	51	178	- ⁺	4.6	3.1
May 24	Bering Sea	01	36	48	57	171	- ⁺	4.7	3.0
May 26	Near Islands	03	20	10	52	175	- ⁺	4.8	2.9
May 27	Aleutian Islands	17	22	43	50	174	35	5.3	6.0
May 28	Rat Island	01	32	00	52	176	58	5.0	4.2
June 1	Fox Islands	03	36	22	54	166W	39	5.7	4.1
June 4	Andreanof Islands	09	39	32	51	175W	- ⁺	5.0	3.4
June 19	Fox Islands	17	07	20	51	172W	47	5.5	3.7
June 27	Rat Island	20	32	55	52	178	21	5.1	4.1
June 29	Andreanof Islands	04	53	20	52	178	- ⁺	5.1	3.8
June 30	Rat Island	19	29	59	52	176	32	5.0	3.8

⁺ Depth not available.

TABLE VIII

EPICENTER AND MAGNITUDE DATA FOR THE SOLOMON ISLANDS EVENTS

<u>Date</u>	<u>Region</u>	<u>Origin Time</u>			<u>Latitude (deg. N)</u>	<u>Longitude (deg. E)</u>	<u>Depth (km)</u>	<u>m_b</u>	<u>M_s</u>
		<u>h</u>	<u>m</u>	<u>s</u>					
1967									
Mar 7	Santa Cruz Islands	17	23	00	07	167	⁺ —	4.8	3.9
Mar 9	South Pacific	03	24	41	05	167	27	5.0	5.1
Mar 9	South Pacific	05	38	42	06	166	33	4.8	4.8
Mar 9	South Pacific	05	52	36	06	166	105	4.9	5.3
Mar 9	South Pacific	05	55	09	06	166	⁺ —	4.8	5.3
Mar 9	South Pacific	06	58	52	06	166	78	5.6	6.1
Mar 9	South Pacific	08	16	55	06	166	40	5.0	5.5
Mar 9	South Pacific	18	03	04	04	167	⁺ —	5.4	6.0
Apr 10	Solomon Islands	21	49	19	07	156	39	5.5	4.8
Apr 12	New Caledonia	13	58	28	25	167	⁺ —	5.2	5.1
Apr 13	New Hebrides	04	14	37	16	171	⁺ —	5.2	3.9
Apr 26	New Hebrides	21	46	06	19	170	2	5.2	4.9
May 17	N. of Solomon Is.	12	57	12	03	157	⁺ —	4.5	4.6
May 17	New Hebrides	16	13	22	16	172	⁺ —	5.2	4.2
June 1	D'Entrecasteaux Is.	20	46	31	08	152	80	5.5	5.2
June 15	S. of Solomon Is.	00	15	10	02	164	⁺ —	4.8	3.3
June 23	Santa Cruz Islands	21	30	41	12	170	36	4.7	4.3
June 26	Loyalty Islands	09	07	57	25	170	⁺ —	5.5	4.2
July 8	New Caledonia	00	58	14	18	161	⁺ —	5.2	4.1
July 12	New Hebrides	21	14	23	19	171	63	5.1	5.1

⁺ Depth not available.

given in Fig. 21(a) - (d) were also plotted vs the U. S. Coast and Geodetic Survey (USCGS) body-wave magnitude, and gave a similar separation between bombs and earthquakes.

The results obtained for the other epicentral regions in Figs. 21(b) - (d) show that these regions give rise to earthquakes for which the M_s vs m_b characteristic is somewhat different from that of the Central Asian area. In fact, the separation between these earthquakes and the Central Asian explosions appears to be worse for these other regions than that found for the Central Asian area. This has also been found to be the case in a recent study of Aleutian earthquakes and the underground nuclear explosion, Longshot,¹² and several other recent works.^{13, 14}

An attempt was made to determine the detection threshold at LASA for LP Rayleigh surface waves for natural seismic events from the Central Asian-Kurile Islands-Kamchatka region. A selection of events from this region, for which pP was not observed on LASA data, from December 1966 to the end of April 1967 were used as a reference population of events. Approximately 53 events were included ranging in body-wave magnitude from 3.7 to 6.5. The P-wave for the events was detected by using a short-period (SP) beam and the Rayleigh surface waves were detected by using a LP beam and matched filtering, as described previously. The results of the experiment are given in Fig. 22, which shows the cumulative distribution of the events detected. It is seen that at $m_b = 4.5, 4.9$ at LASA, 60, 100 percent detectability of Rayleigh surface waves is achieved, respectively. As mentioned previously, a threshold 6 db above the noise level at the output of the matched filter, and at the appropriate

arrival time for surface waves, was required before the detection of an event was claimed. At this threshold there is about 10 percent probability that a noise pulse has exceeded the threshold, as indicated in Appendix B. A corresponding detectability result for the underground nuclear explosions is difficult to give at this point due to the small number of such events for which both SP and LP data at LASA are available. However, according to Fig. 21(a), Rayleigh surface waves have been detected for underground nuclear explosions whose body-wave magnitude is as low as 5.3.

VI. CONCLUSIONS

It has been found that the most useful LP phase for the purpose of discriminating between earthquakes and underground nuclear explosions is the Rayleigh surface wave. This is true because it is the only phase seen at teleseismic distances for small magnitude events. This phase provides the information necessary to compute the surface-wave magnitude, which in conjunction with the body-wave magnitude, has proved to be the discriminant which leads to a clear separation between the two populations. In addition, this discriminant can be applied at lower magnitude levels than any which are based for example on LP body-wave phases such as P- and S-waves. The LPZ sensors have been found to have about 10 db lower noise level than the EW, NS components. Thus, for the purpose of seismic discrimination it is only the LP Rayleigh surface waves and the LPZ sensors which have been found to be important.

The DS-MF form of processing was found to have a total SNR gain in the signal frequency band of about 19 db. This type of signal processing has the advantages of simplicity of implementation and relative immunity to such anomalies as weak sensors and spurious spikes in the data. It is possible to achieve somewhat more SNR gain with the MF-FS and BP-FS-MF forms of processing. However, this additional gain, which is usually about 3 db, must be obtained with FS processing which has the disadvantages of complex implementation and extreme vulnerability to anomalies such as weak sensors. An analyst should, in applying this processing, delete weak traces, as mentioned previously. It may also take several digital computer runs before it can be

ascertained that the appropriate traces have been deleted. This procedure can be very complicated and expensive considering the small improvement in SNR gain which is obtained relative to the simpler DS-MF form of processing. The conclusion, therefore, is that certainly for on-line processing of Rayleigh surface waves the form of processing to be used should be DS-MF. For off-line processing DS-MF processing also appears to be adequate, with possibly a small role for MF-FS processing for extremely weak events. In other words, the DS-MF processing should play the major role in both off-line and on-line processing.

In order to make the DS-MF processing as effective as possible, the LPZ sensors should be placed about 30 km apart. This minimum separation between sensors has been shown, on the basis of noise data from the Montana LASA, to provide SNR gain for DS processing which is within 1 db of the $10 \log_{10} NS$ to be obtained for independent noise. Thus, the optimum LP array geometry for the purpose of seismic discrimination should consist of LPZ sensors positioned with a minimum separation of about 30 km between seismometers. This assumes that the beamforming gain pattern of the array has no severe sidelobes which will allow significant amounts of off-angle noise to pass without attenuation. In order to prevent significant dispersion across the array, it appears that the maximum array diameter should be about 200 km. However, it is possible that the dispersion for an array of larger diameter than 200 km can be corrected by the use of say appropriately matched filters, to allow beamforming to take place without significant signal loss. Pending the outcome of such an experiment, it would appear tentatively that a maximum LP array diameter of 200 km is desirable.

It should be stressed that the SNR gain of DS-MF will be close to $10 \log_{10} NS$, with suitably separated sensors, if the azimuth of the event is different from that of a coherent noise source by about plus or minus one-half the beamwidth, the beamwidth of the 200 km LASA is about 40 degrees for the LP Rayleigh waves. Thus, if the azimuth of the event is within ± 20 degrees of that of the noise source, the SNR gain at LASA of DS-MF will decrease as indicated previously. Therefore, a noise survey at a proposed new site for the installation of another array is extremely important. Such a noise survey should establish that the azimuth of the noise source will not be within plus or minus a half-beamwidth of the azimuth for those epicentral regions of interest. This is an extremely important point which should be emphasized.

One area in which FS processing has been found to be more useful than DS processing is in the suppression of interfering LP surface waves. Therefore, FS processing should serve a purpose off-line for processing those events which have been obscured by an interfering LP event. It is interesting to note how organized in frequency-wavenumber space the interfering event must be before FS processing achieves significant SNR gain relative to DS processing. Although the LP noise is organized in frequency-wavenumber space, there is not sufficient organization to allow a significant advantage for FS over DS processing

The matched filtering of LP surface waves can be accomplished by using chirp waveforms. The initial and final periods of the chirp waveform should be 40 and 20 seconds, respectively. The length of the chirp waveform should be adjusted for the best match, as indicated previously.

An extensive study of the $M_s - m_b$ characteristic for earthquakes from four tectonic regions of the earth has been made. In addition, a similar study has been made for presumed underground nuclear explosions for Central Asia. The results show a distinct separation between the two populations. The body-wave magnitude at LASA at which 100 percent detectability of LP Rayleigh surface waves is obtained is 4.9, while 60 percent detectability is achieved at magnitude 4.5, for natural seismic events from the Central Asian-Kurile Islands-Kamchatka region.

APPENDIX A

DERIVATION OF SIGNAL-TO-NOISE RATIO GAIN OF MATCHED FILTERS USING CHIRP WAVEFORMS

We assume that the input signal sequence is a chirp waveform given by

$$S_k = A \sin \left\{ 2\pi f_0 kT + \frac{1}{2} [2\pi(f_1 - f_0) \left(\frac{k-1}{N-1}\right) kT] \right\}, \quad k = 1, \dots, N \quad (1)$$

where f_0, f_1 are the initial and final frequencies, in Hz, respectively, T is the sampling interval in seconds and N is the number of points in the input signal sequence. The total processing time L is given by

$$L = NT \quad (2)$$

and the bandwidth W is

$$W = f_1 - f_0 \quad (3)$$

The actual value used for A was 0.01, but for simplicity, and with no loss of generality, we will assume here that $A = 1$. The signal sequence S_k is, of course, the same as the reference waveform used to crosscorrelate with the signal plus noise data. The input noise is assumed to be white over the signal frequency band with a sampled power spectrum given by

$$N(f) = \frac{N_0}{2} \text{ watts/Hz, } f_0 \leq |f| \leq f_1$$

$$= 0, \text{ otherwise}$$

in the frequency range $|f| \leq \frac{1}{2T}$.

The input noise power is

$$N_{IN} = \int_{-1/2T}^{1/2T} N(f) df$$

$$= N_0 W . \quad (4)$$

The peak input signal is

$$S_{IN} = 1 \quad (5)$$

and the peak output signal is

$$S_{OUT} = \sum_{k=1}^N S_k^2 \cong \frac{N}{2} . \quad (6)$$

The output noise power is

$$N_{OUT} = \int_{-1/2T}^{1/2T} |S(f)|^2 g(f) df , \quad (7)$$

where

$$S(f) = \sum_{k=1}^N S_k e^{i2\pi f k T} \quad (8)$$

so that

$$\begin{aligned} N_{\text{OUT}} &\cong \frac{N_0}{2} \int_{-1/2T}^{1/2T} |S(f)|^2 df \\ &= \frac{N_0}{2} \frac{1}{T} \sum_{k=1}^N S_k^2 \\ &\cong \frac{N_0 N}{4T} \end{aligned} \quad (9)$$

Thus, the SNR gain, G , is

$$G = \frac{S_{\text{OUT}}^2 / N_{\text{OUT}}}{S_{\text{IN}}^2 / N_{\text{IN}}} \quad (10)$$

so that using Eqs. (5), (6), (7), and (9) we have

$$\begin{aligned} G &= NTW = LW \\ &= \text{TIME - BANDWIDTH PRODUCT} \quad . \end{aligned} \quad (11)$$

Hence, if the input signal were a chirp waveform, then the SNR gain obtained by a matched filter would be equal to the time-bandwidth product.

Suppose now that the input signal is no longer a true chirp waveform but a chirp waveform with a nonuniform envelope whose peak value is unity. The optimum filter is one which crosscorrelates the signal plus noise data with the reference sequence matched to the signal sequence S'_k . We now wish to compute the SNR gain, G' , provided by the optimum filter in this case. The values for S_{IN} and N_{IN} remain the same as those given in Eqs. (5) and (4), respectively. The peak signal output is now given by

$$\begin{aligned} S'_{OUT} &= \sum_{k=1}^N (S'_k)^2 \\ &\cong \frac{1}{2} \sum_{k=1}^N E_k^2 \end{aligned} \quad (12)$$

where E_k are the values of the envelope of the signal sequence and $\text{MAX}_{1 \leq k \leq N} E_k = 1$, $0 \leq E_k \leq 1$. The output noise power is

$$\begin{aligned} N'_{OUT} &\cong \frac{N_0}{2T} \sum_{k=1}^N (S'_k)^2 \\ &\cong \frac{N_0}{4T} \sum_{k=1}^N E_k^2 \end{aligned} \quad (13)$$

Thus the SNR gain, G' , is

$$G' = \frac{(S'_{OUT})^2 / N'_{OUT}}{S_{IN}^2 / N_{IN}} \quad (14)$$

which by Eqs. (4), (5), (12), (13) is

$$G' = B L W \quad (15)$$

$$= \text{equivalent time-bandwidth product}$$

where

$$B = \frac{1}{N} \sum_{k=1}^N E_k^2 \quad (16)$$

It should be noted that $0 < B \leq 1$, so that the effect of the nonuniform envelope of the signal is to reduce the SNR gain, below the value given by the time-bandwidth product, by the factor B .

We now wish to calculate the loss of SNR gain due to the mismatch caused by using a chirp waveform for matched filtering when the signal actually has a nonuniform amplitude. The peak signal output now is

$$S''_{\text{OUT}} = \sum_{k=1}^N S_k S'_k = \sum_{k=1}^N S_k^2 E_k$$

$$\cong \frac{1}{2} \sum_{k=1}^N E_k \quad (17)$$

The values of S_{IN} , N_{IN} remain the same as those given in Eqs. (5) and (4), respectively, and the value of N_{OUT} is given by Eq. (9). The SNR gain, G'' , in this case is given by

$$G'' = \frac{(S''_{\text{OUT}})^2 / N_{\text{OUT}}}{(S_{\text{IN}}^2) / N_{\text{IN}}} \quad (18)$$

so that using Eqs. (4), (5), (9), and (17) we get

$$G'' = C L W = \frac{C}{B} G' \quad (19)$$

where

$$C = \left(\frac{1}{N} \sum_{k=1}^N E_k \right)^2 . \quad (20)$$

Thus, the effect of using a chirp waveform as a matched filter reference for a signal with nonuniform envelope is to lower the SNR gain below the optimum value G' by the ratio C/B , which is positive and must, by the Schwarz inequality, be always less than or equal to unity, i. e., $0 < C/B \leq 1$. The quantities B and C have been measured for several events and $10 \log_{10}(B/C)$ is usually only a few tenths of a db. Thus, we obtain the important result that the use of a chirp waveform for matched filtering of signals with nonuniform envelopes entails a loss of only a few tenths of a db.

APPENDIX B

COMPUTATION OF PROBABILITY OF NOISE EXCEEDING A SPECIFIED THRESHOLD

We now wish to compute the probability that the envelope of the noise at the output of the matched filter exceeds a specified threshold during a given time interval. It is assumed that the bandwidth of the noise is W Hz and that independent noise envelope samples are generated every $1/W$ seconds. The total number of noise envelope samples is assumed to be M and they will be denoted by X_1, \dots, X_M and assumed to be identically distributed. The required probability is

$$P_N(X) = \text{Prob} \left\{ \text{MAX}_{\{1 \leq k \leq M\}} \{X_k\} \geq X \right\}$$
$$= 1 - F^M(X)$$

where X is the specified threshold and $F(u)$ is the cumulative distribution function of X_k , $k = 1, \dots, M$.

The following form for $F(X)$ is assumed

$$F(X) = 1 - e^{-X^2/2\sigma^2}, \quad X \geq 0$$
$$= 0, \quad X < 0$$

where σ is the root-mean-square level of the noise, cf. reference 15, p. 160. Thus

$$P_N(X) = 1 - (1 - e^{-X^2/2\sigma^2})^M, \quad X \geq 0$$

$$= 1, \quad X < 0.$$

The probability $P_N(X)$ is shown plotted vs X/σ in Fig. 23(a) for $W = 1/40$ Hz. In order to check the validity of the assumptions a digital computer program was developed to measure $P_N(X)$ experimentally on the noise data. The results are given in Fig. 23(b) which shows reasonably good agreement with the theoretical results given in Fig. 23(a).

Ordinarily the arrival of the compressed surface wave signal at the output of the matched filter is known to within 40 seconds, so that if a threshold-to-rms noise level of 6 db is maintained at the output of the matched filter, there will be about 10 percent probability that a noise pulse alone exceeded the threshold, as seen from Fig. 23(a). If an amplitude of A is observed at the output of the matched filter, under these conditions, then there is about 90 percent probability that the true signal amplitude is between $(A - 2\sigma)$ and A , assuming that cumulative distribution function of signal plus noise is the same as that of noise except for a simple translation. In other words, only a probability confidence limit statement can be made concerning the true signal amplitude when the signal-to-noise ratio is near unity. For simplicity, in the present work the amplitude of the matched filter output has been taken as equal to the true signal output. Of course, if $A \gg \sigma$, then there is very little error introduced by this simplifying assumption.

REFERENCES

1. P. E. Green, R. A. Frosch and C. F. Romney, "Principles of an Experimental Large Aperture Seismic Array (LASA)," Proc. IEEE, 53, December 1965.
2. J. Capon, R. J. Greenfield, R. J. Kolker and R. T. Lacoss, "Short-Period Signal Processing Results for the Large Aperture Seismic Array," to be published in Geophysics.
3. J. Capon, R. J. Greenfield, and R. J. Kolker, "Multidimensional Maximum-Likelihood Processing of a Large Aperture Seismic Array," Proc. IEEE, 55 February 1967.
4. J. R. Klauder, A. C. Price, S. Darlington, and W. J. Albersheim, "The Theory and Design of Chirp Radars," Bell System Technical Journal, 39, July 1960.
5. S. S. Alexander and D. B. Rabenstine, "Detection of Surface Waves From Small Events at Teleseismic Distances," Seismic Data Laboratory Report No. 175, 1 March 1967.
6. K. Aki, "Study of Earthquake Mechanism by a Method of Phase Equalization Applied to Rayleigh and Love Waves," J. Geophys. Res., 65, February 1960.
7. V. I. Keilis-Borok, "Differences in the Spectra of Surface Waves from Earthquakes and from Explosions," Tr. Inst. Fiz. Zemli, 182, 1961.
8. F. Press, G. Dewart and R. Gilman, "A Study of Diagnostic Techniques for Identifying Earthquakes," J. Geophys. Res., 68, May 1963.
9. J. N. Brune, A. Espinosa and J. Oliver, "Relative Excitation of Surface Waves by Earthquakes and Underground Explosions in the California-Nevada Region," J. Geophys. Res., 68, June 1963.
10. B. Gutenberg and C. F. Richter, "Magnitude and Energy of Earthquakes," Ann. Geophys., 9, 1956.
11. B. Gutenberg, "Amplitudes of Surface Waves and Magnitudes of Shallow Earthquakes," Bull. Seismol. Soc. Am., 35, 1945.

12. R. C. Lieberman, C. Y. King, J. N. Brune and P. W. Pomeroy, "Excitation of Surface Waves by the Underground Nuclear Explosion Longshot," *J. Geophys. Res.*, 71, September 1966.
13. P. D. Marshall, E. W. Carpenter, A. Douglas, and J. B. Young, "Some Seismic Results of the Longshot Explosion," Rept. 0-67/66, Atomic Weapons Research Establishment, U. K. Atomic Energy Authority, 1966.
14. R. C. Liebermann, and P. W. Pomeroy, "Excitation of Surface Waves by Events in Southern Algeria," *Science*, 156, 26 May 1967.
15. W. L. Davenport, Jr., and W. L. Root, Random Signals and Noise (McGraw-Hill Book Co., New York; 1958).

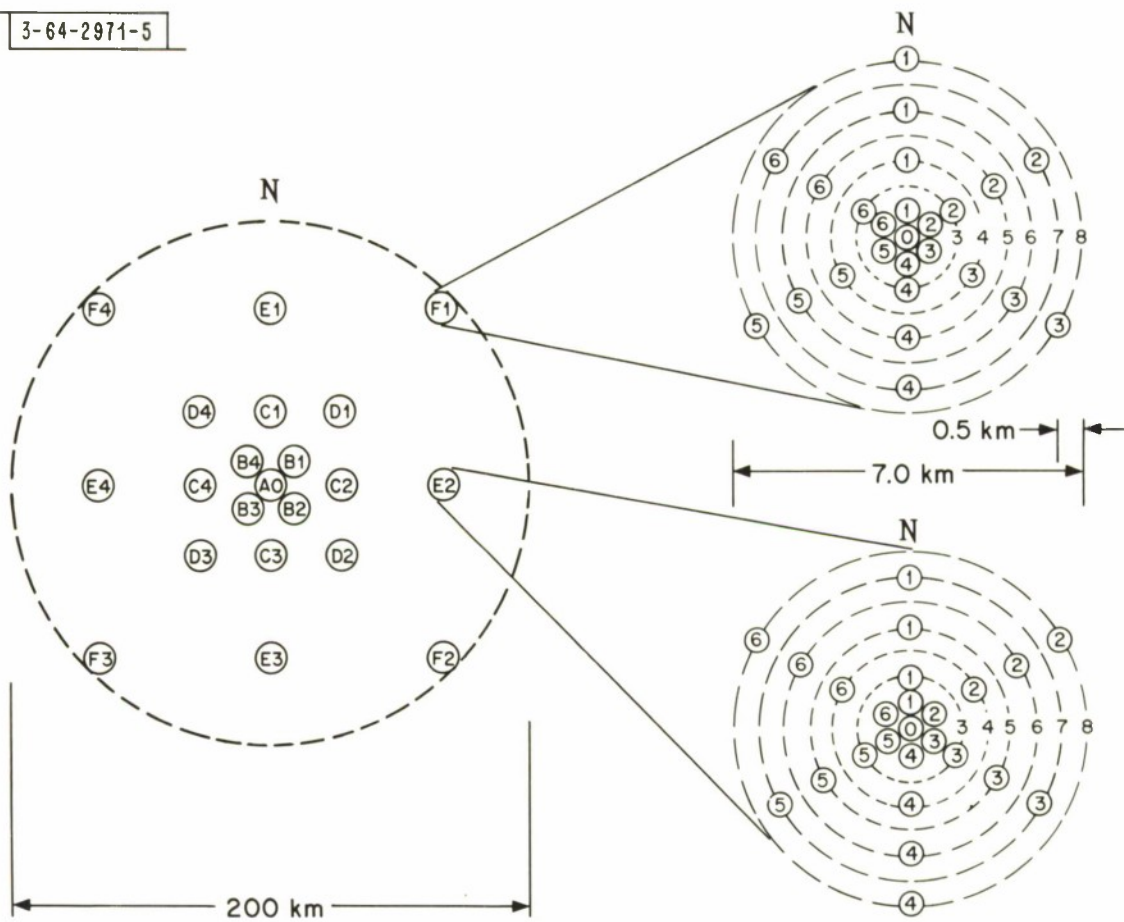
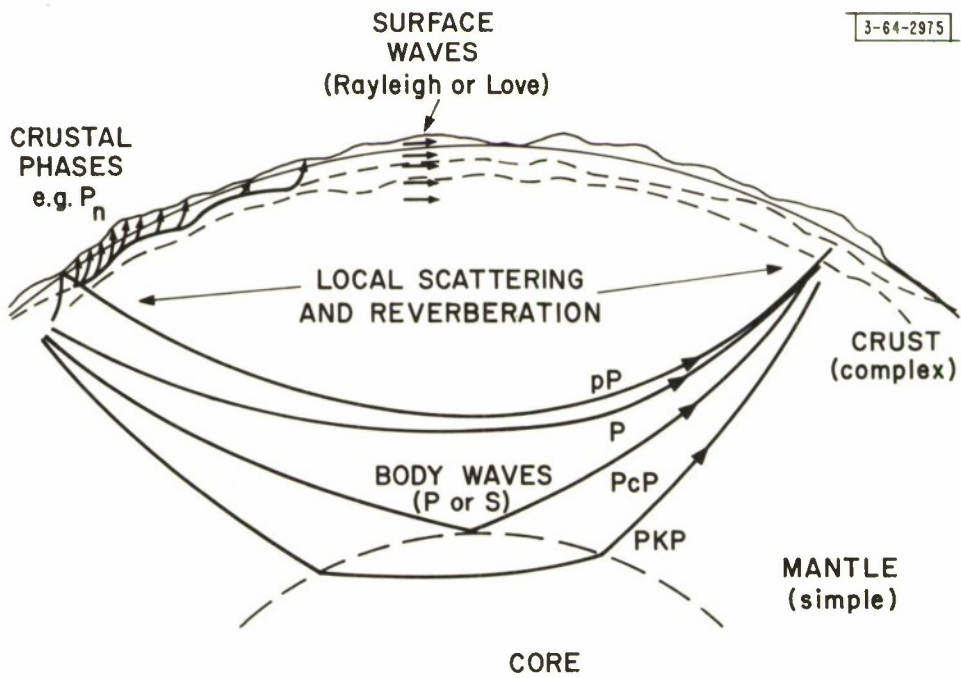
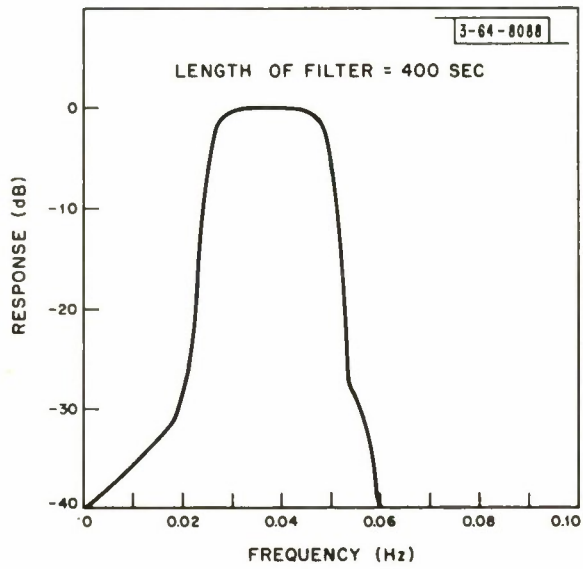


Fig. 1. General arrangement of the large aperture seismic array.

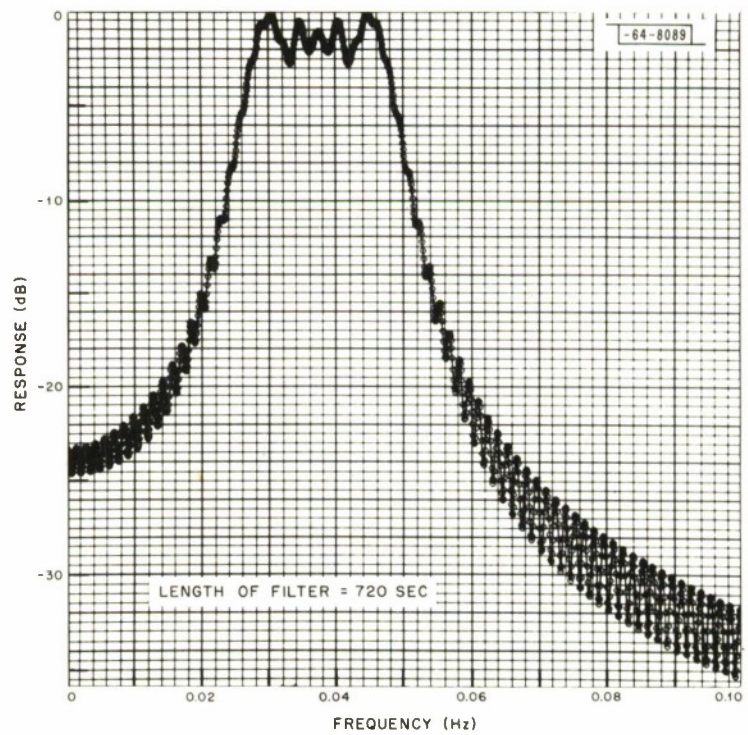


3-64-2975

Fig. 2. Modes of propagation of seismic waves.



(a)



(b)

Fig. 3. Frequency response of (a) 400-second bandpass convolutional filter; (b) 720-second matched filter.

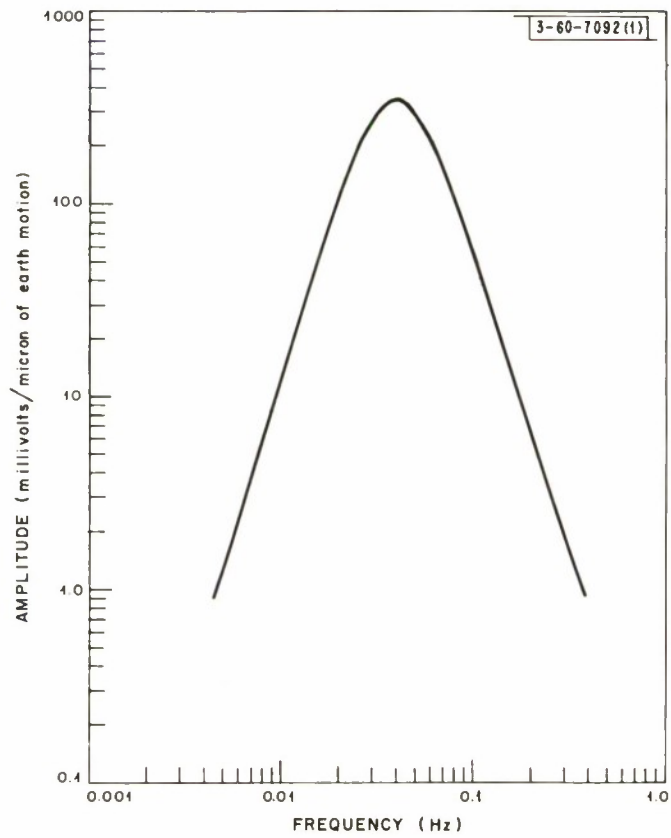


Fig. 4. Long-period system transfer function (25-second filter).

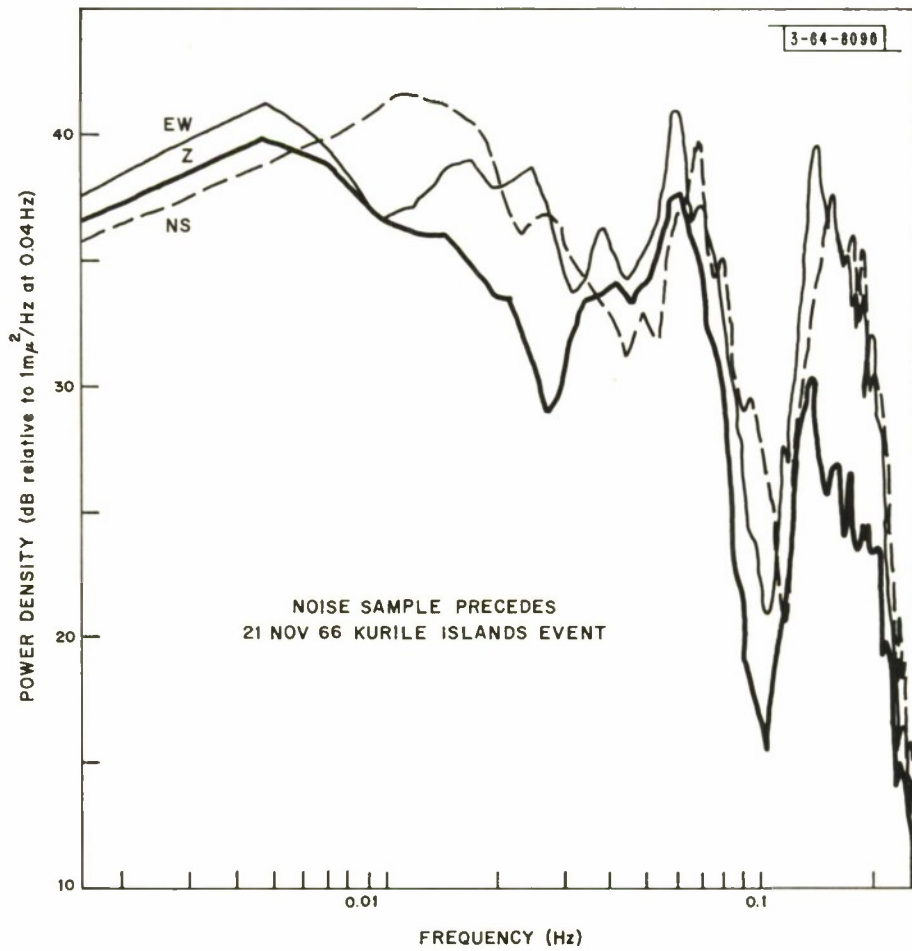


Fig. 5. Power density of long-period noise.

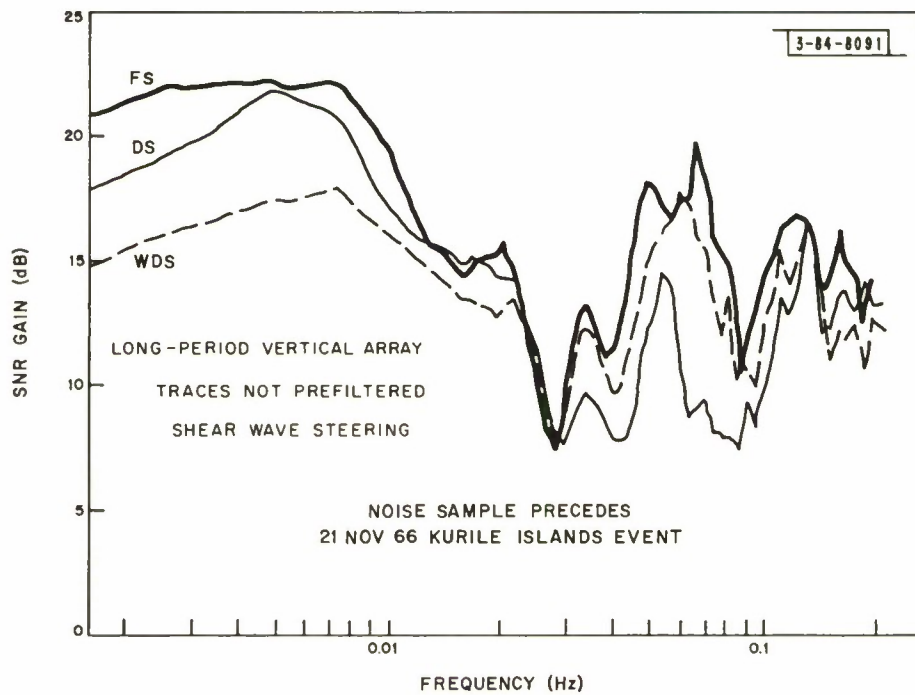


Fig. 6. Signal-to-noise ratio gain of FS, WDS, DS for long-period vertical array using shear wave steering parameters and no prefiltering.

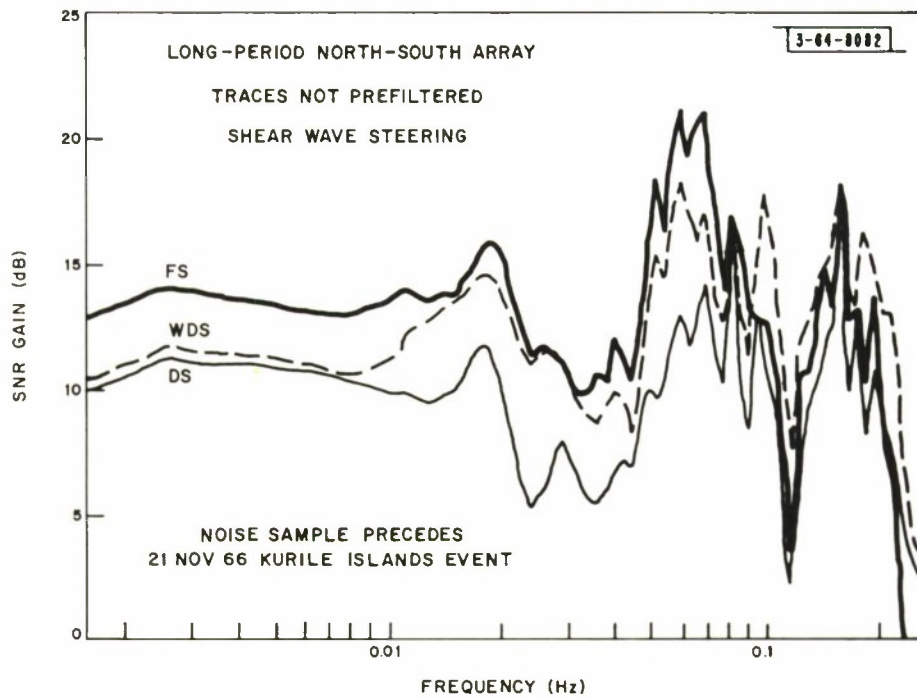


Fig. 7. Signal-to-noise ratio gain of FS, WDS, DS for long-period north-south array using shear wave steering parameters and no prefiltering.

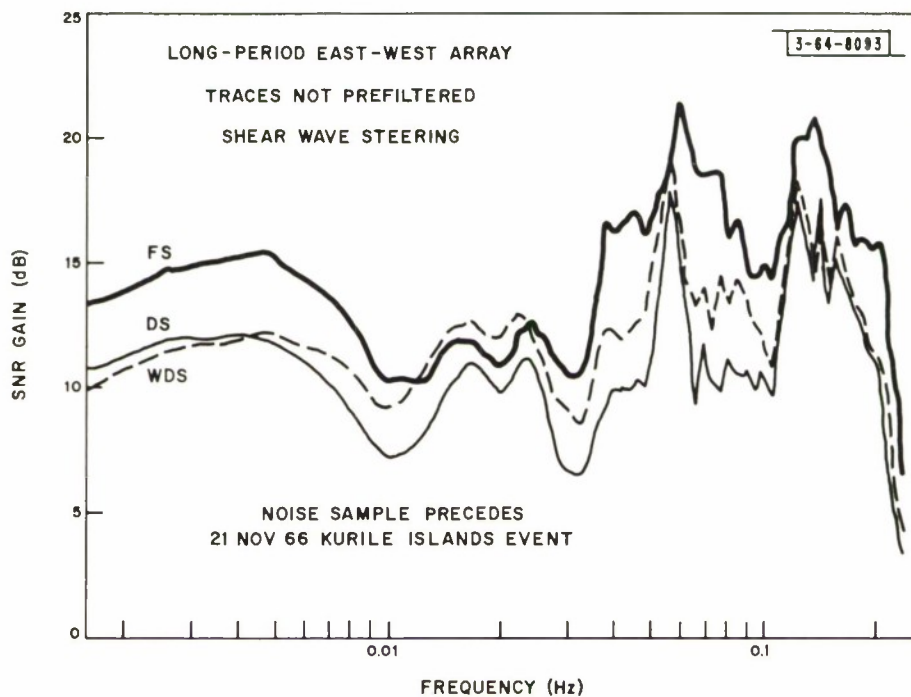


Fig. 8. Signal-to-noise ratio gain of FS, WDS, DS for long-period east-west array using shear wave steering parameters and no prefiltering.

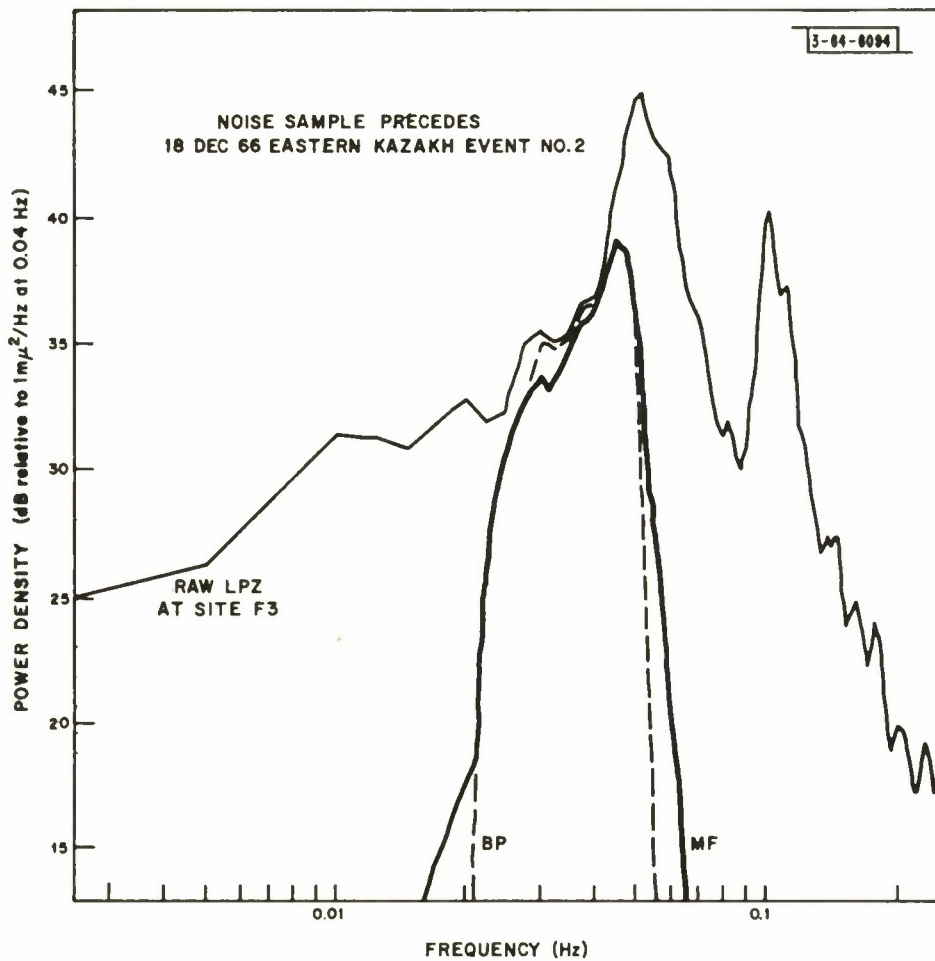


Fig. 9. Power density for raw, bandpass, and matched filtered, long-period vertical noise sample.

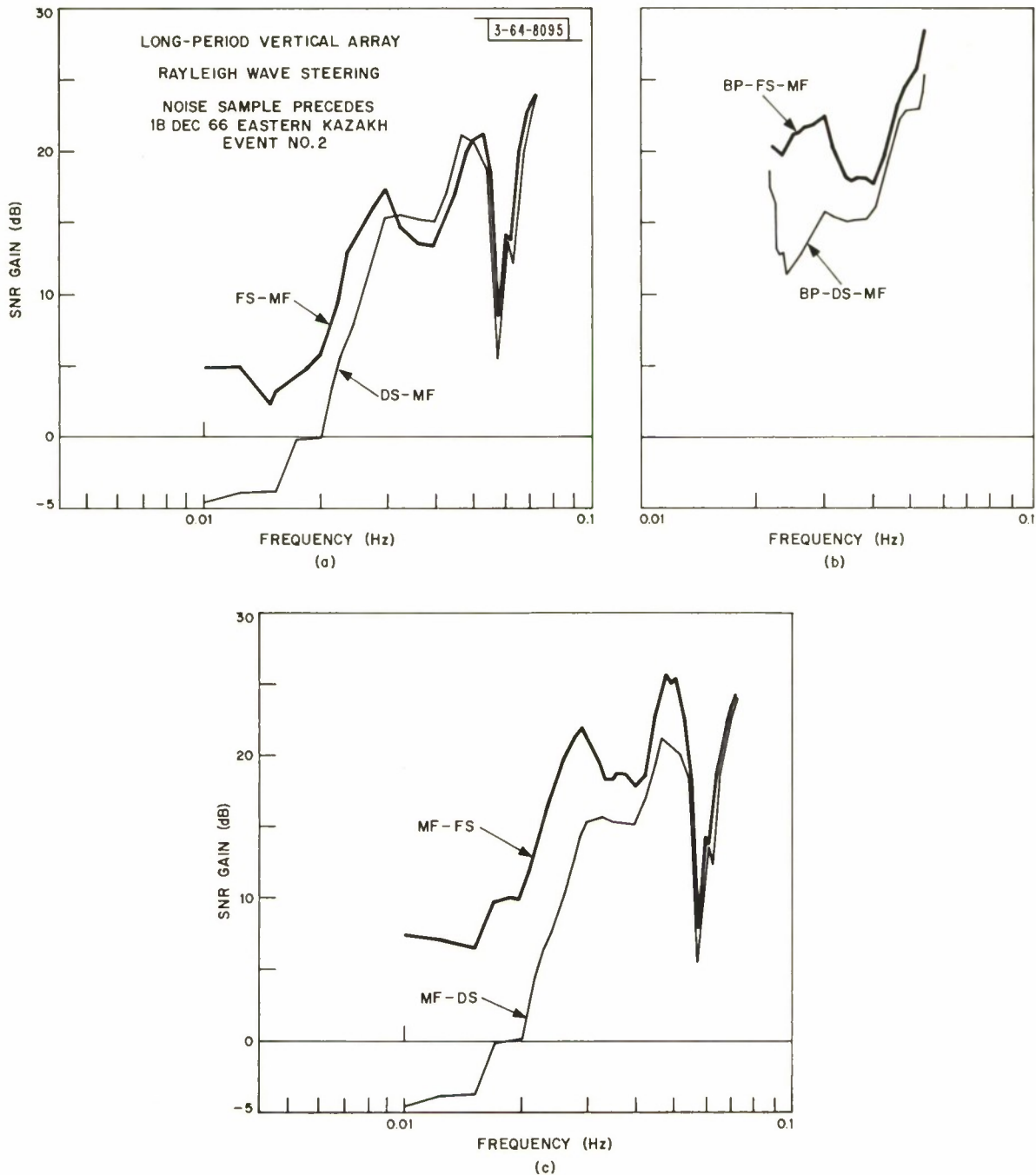
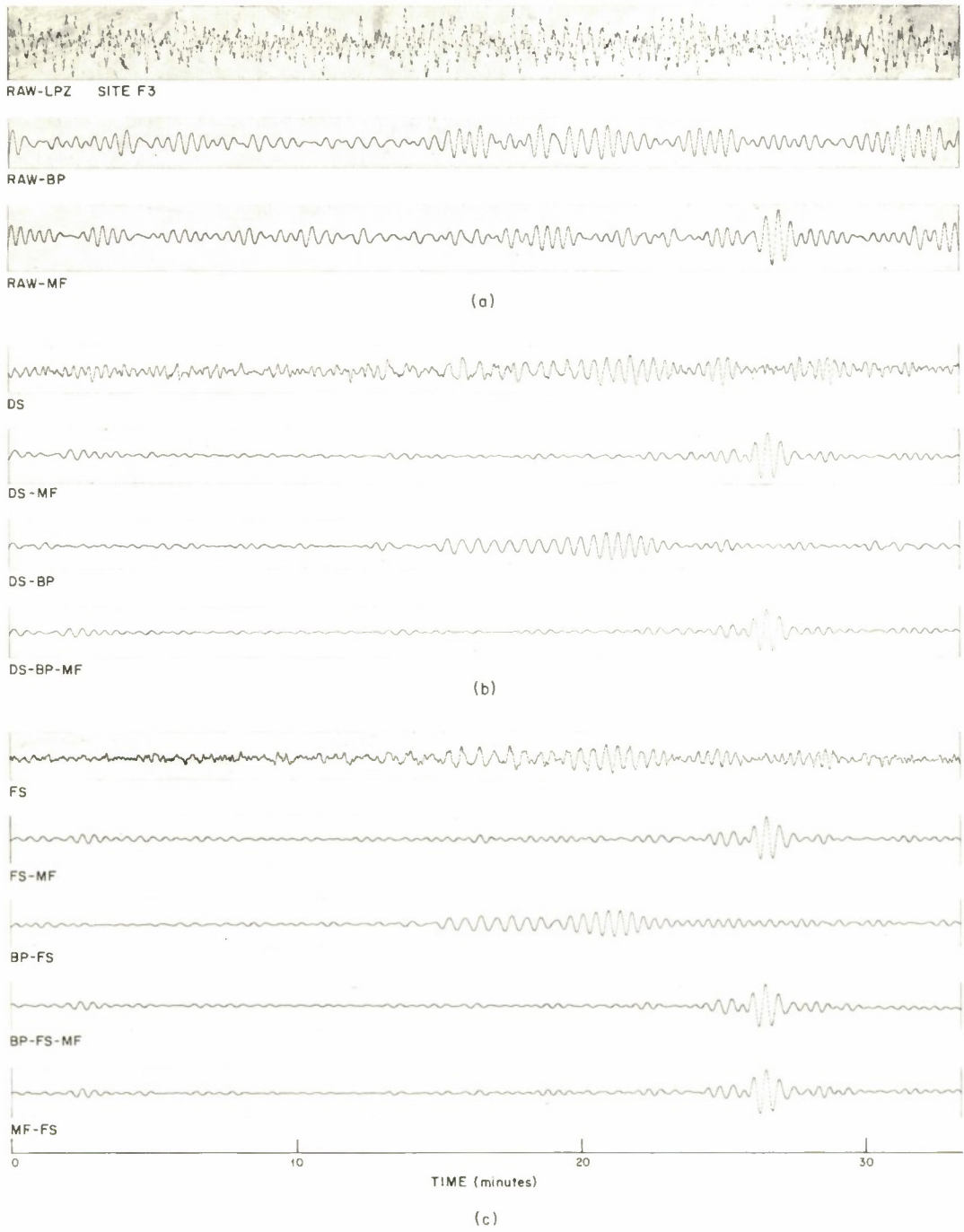


Fig. 10. Signal-to-noise ratio gain for long-period vertical array using Rayleigh wave steering parameters: (a) DS - MF, FS - MF; (b) BP - DS - MF, BP - FS - MF; (c) MF - DS, MF - FS.



18 DEC 66 EASTERN KAZAKH EVENT NO. 2

Fig. 11. Signal-to-noise ratio gain obtained with various forms of processing for long-period vertical array using Rayleigh wave steering parameters.

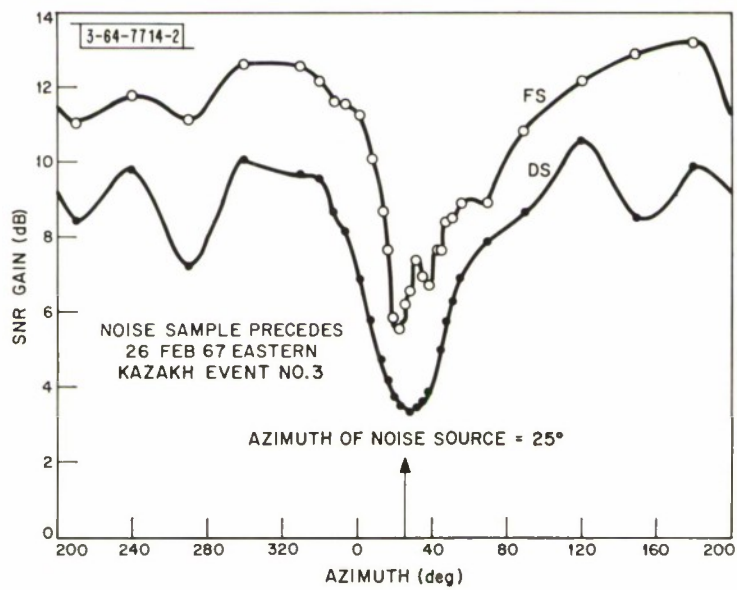


Fig. 12. Signal-to-noise ratio gain of FS, DS vs azimuth for long-period vertical A, D and E rings using Rayleigh wave steering parameters.

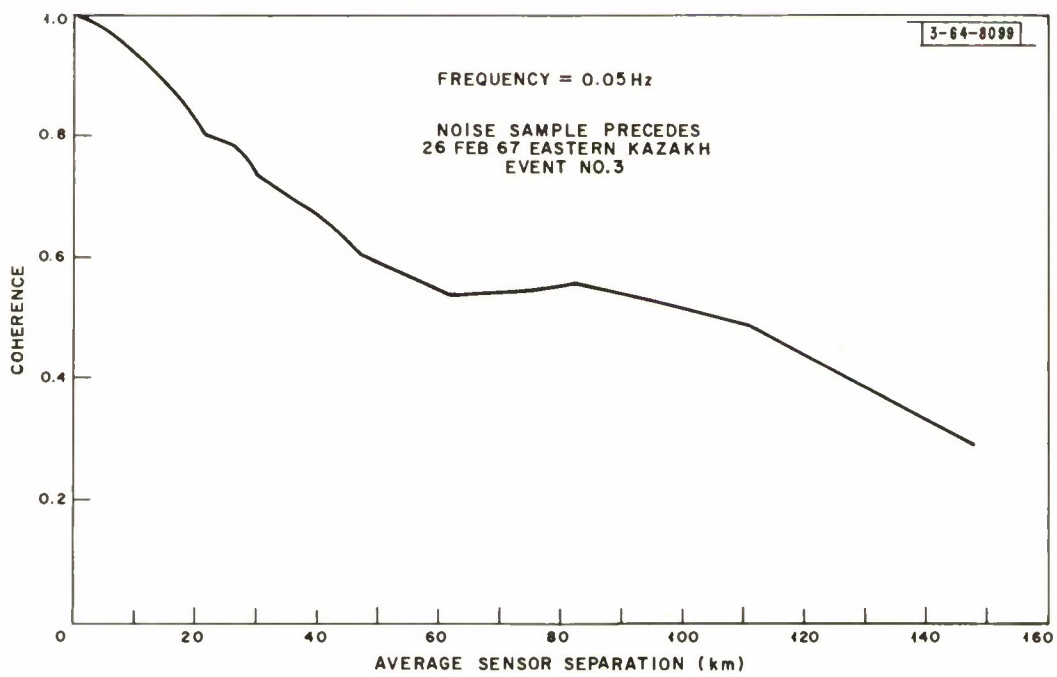


Fig. 14. Coherency vs sensor separation for long-period vertical noise at 0.05 Hz.

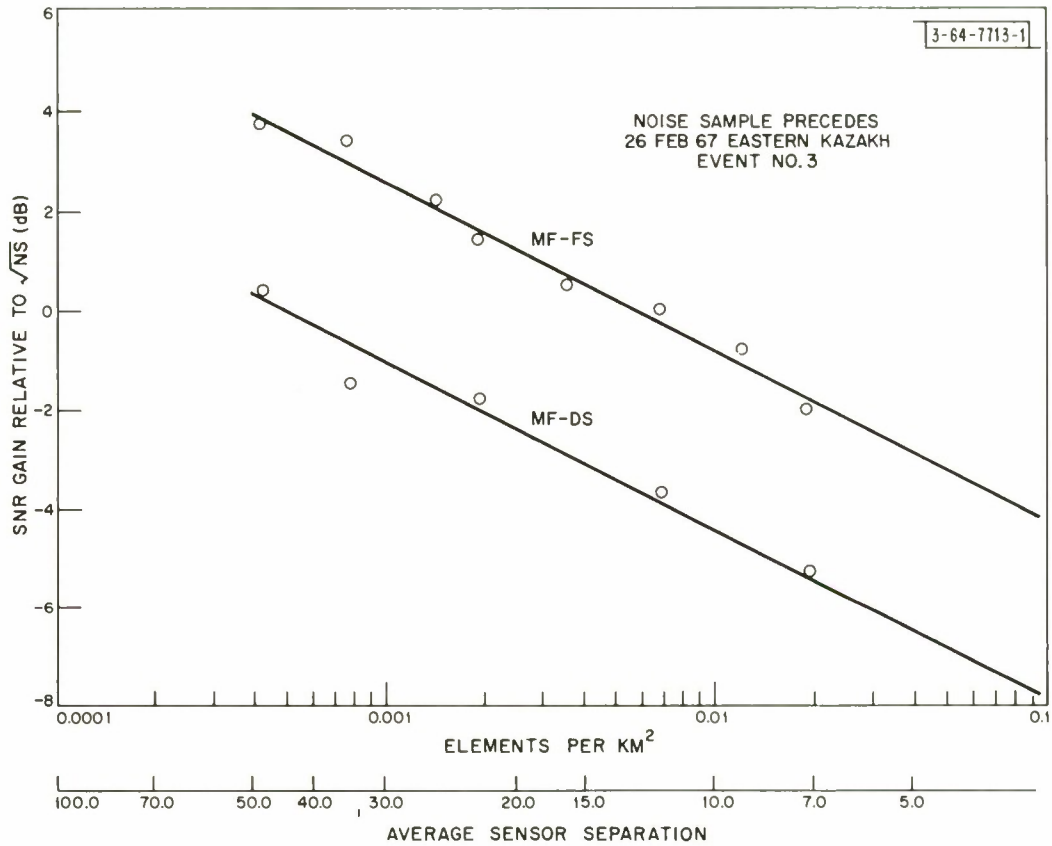


Fig. 15. Signal-to-noise ratio gain relative to \sqrt{NS} of MF - DS, MF - FS, vs element density for long-period vertical array using Rayleigh wave steering parameters.

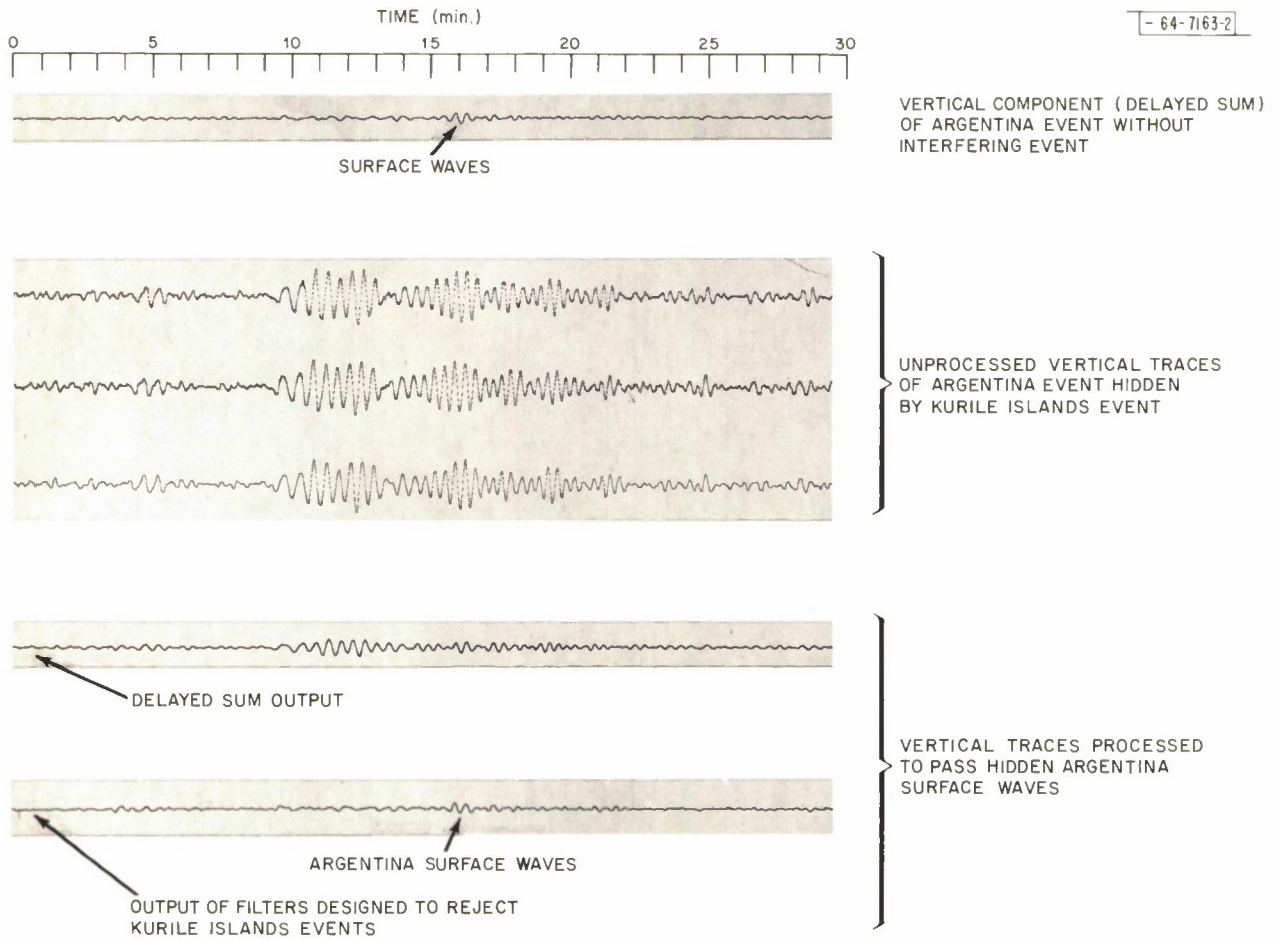


Fig. 16. Suppression of long-period interfering teleseism.

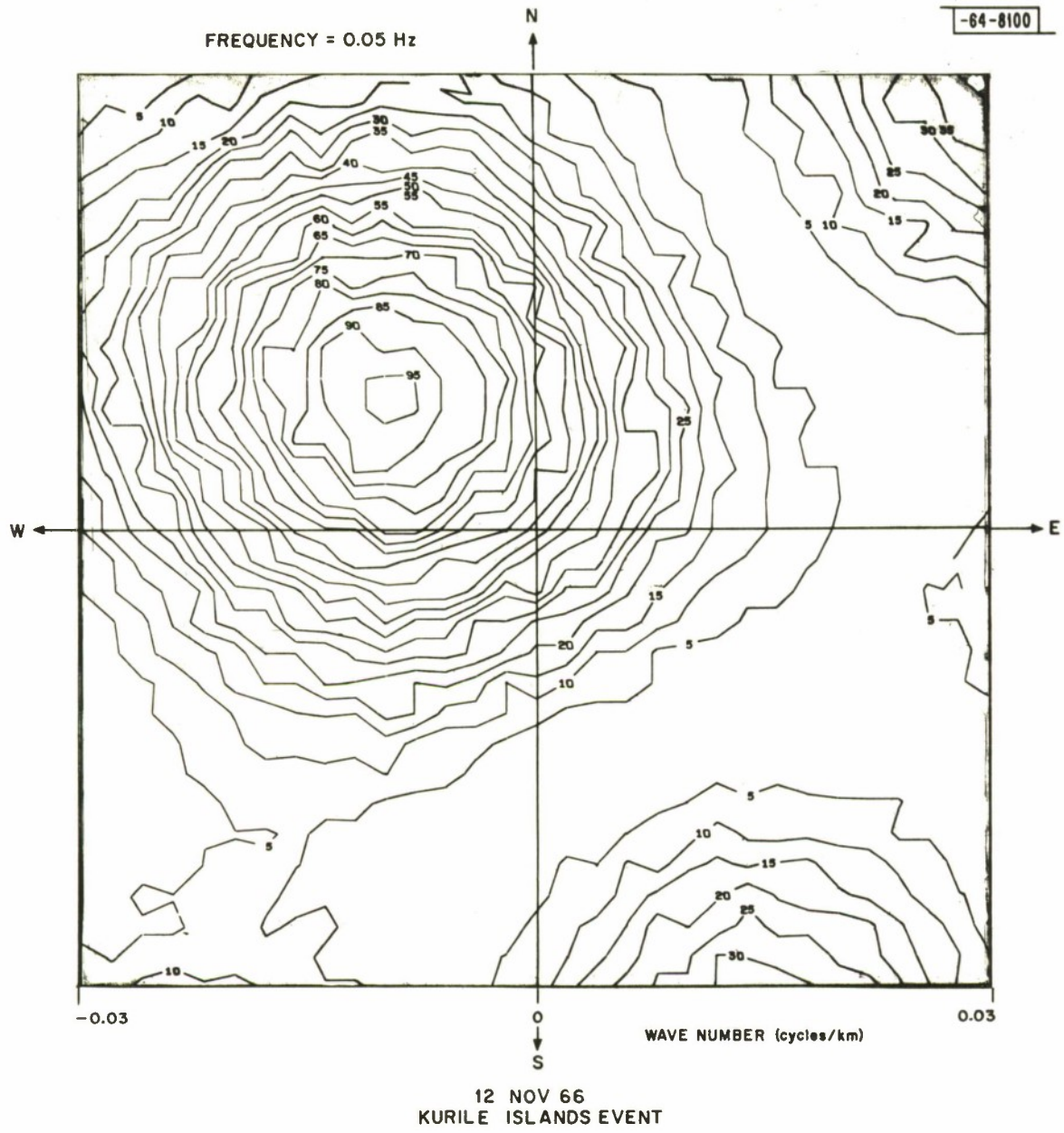


Fig. 17. (a) Wavenumber spectrum of 11/12/66 Kurile Islands event at 0.05 Hz using A, C rings.

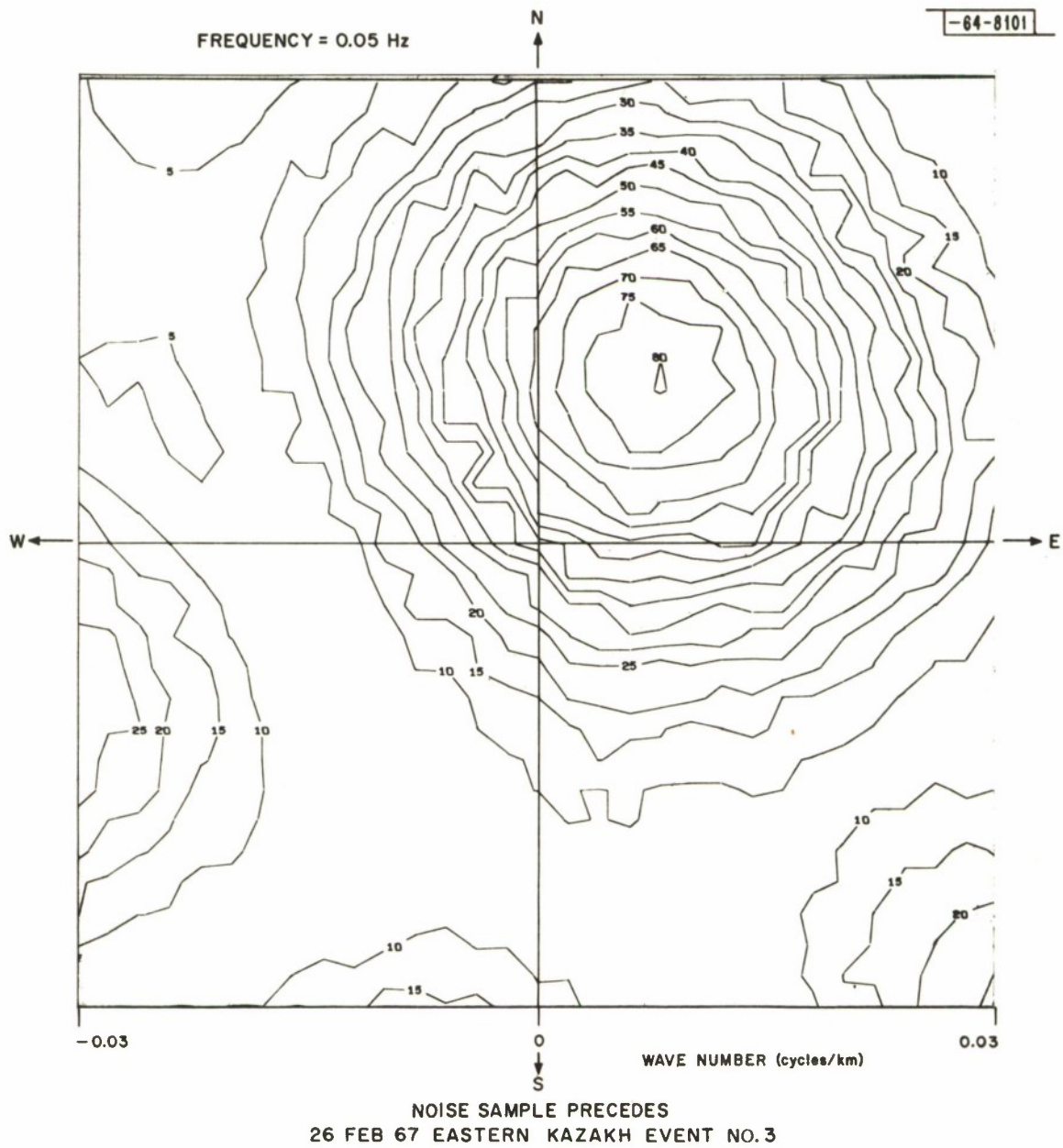


Fig. 17. (b) Wavenumber spectrum of 2/26/67 noise sample at 0.05 Hz using A, C rings.



Fig. 18. Matched filter signal-to-noise ratio improvement for long-period Rayleigh waves.

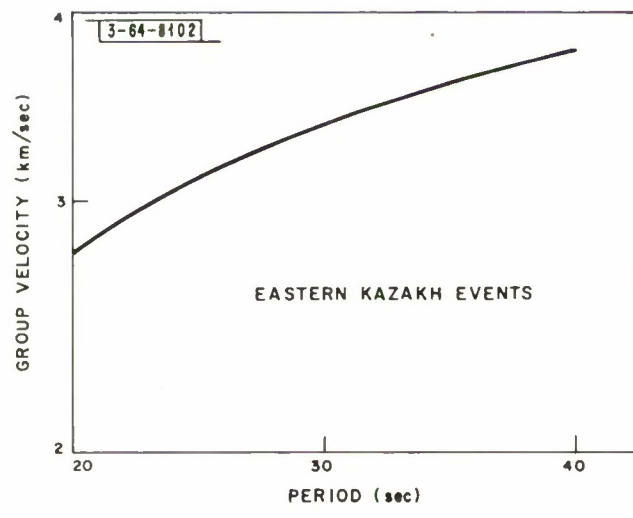
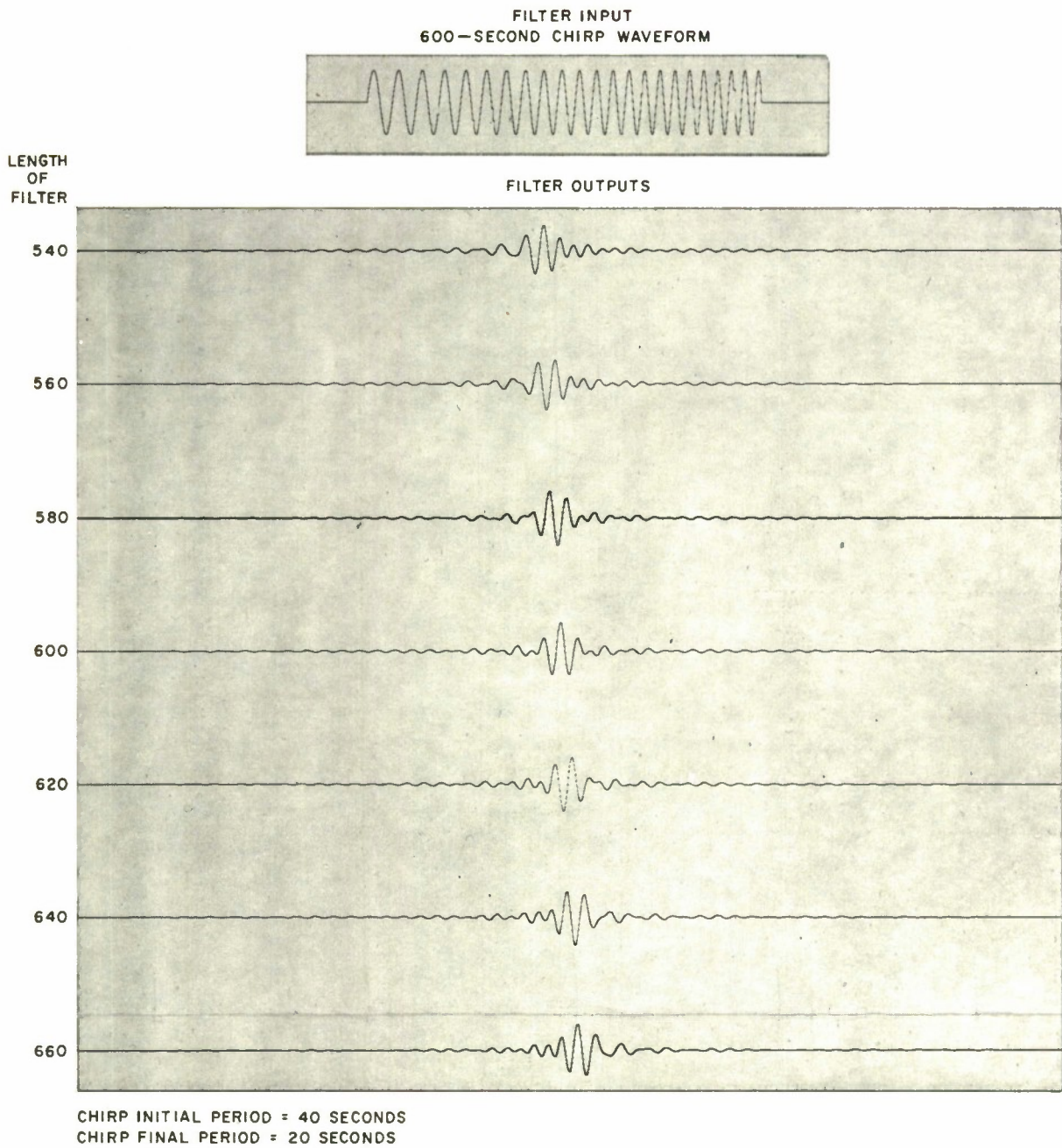


Fig. 19. Group velocity vs period for Eastern Kazakh events.



(a)

Fig. 20. (a) Output of various chirp filters when input is 600 second chirp waveform.



CHIRP INITIAL PERIOD = 40 SECONDS
CHIRP FINAL PERIOD = 20 SECONDS

18 DEC 66 EASTERN
KAZAKH EVENT NO.2

(b)

Fig. 20. (b) Output of various chrip filters when input is a long-period vertical beam.

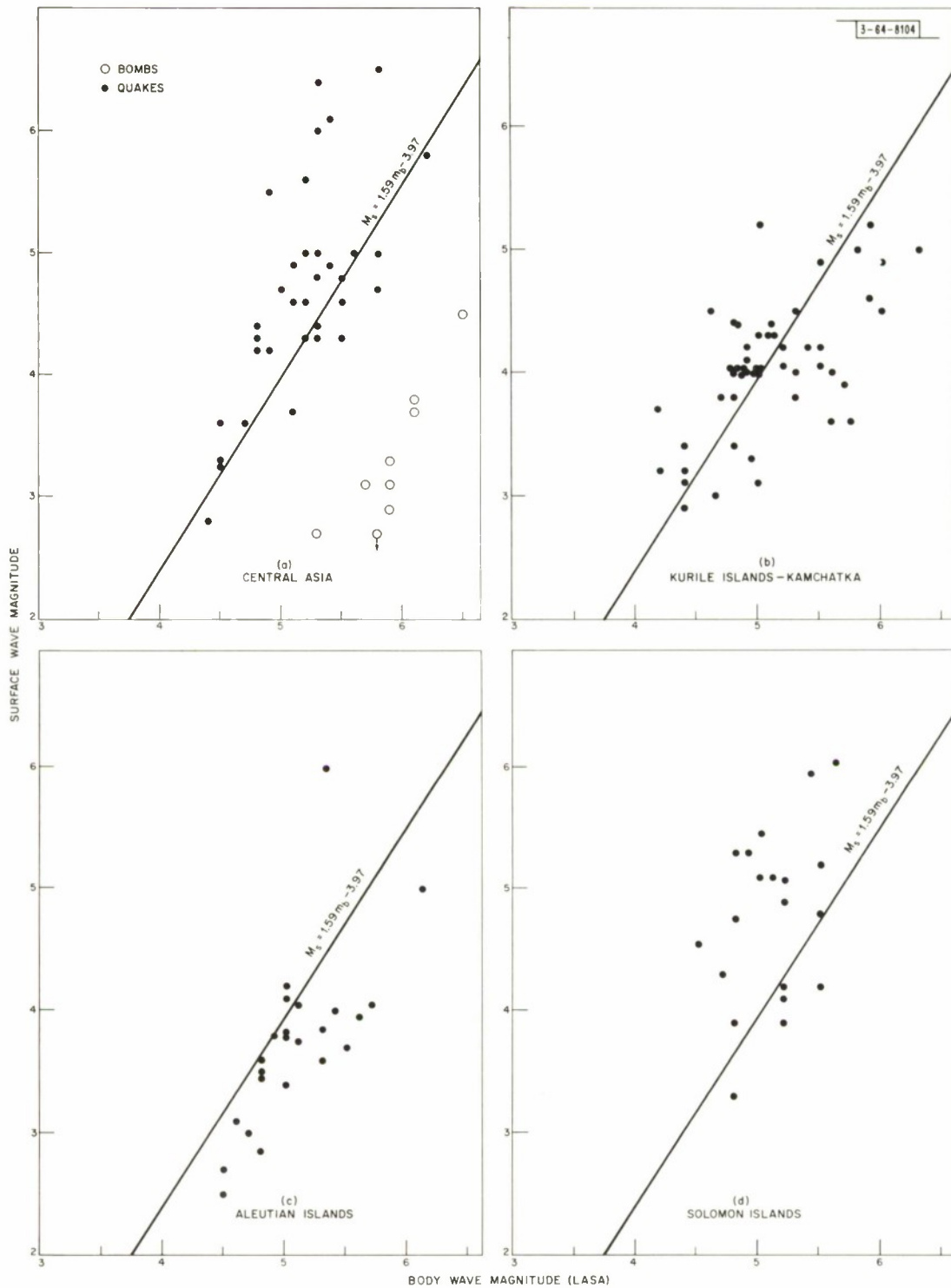


Fig. 21. LASA surface-wave vs body-wave magnitude for events from four tectonic regions of the earth.

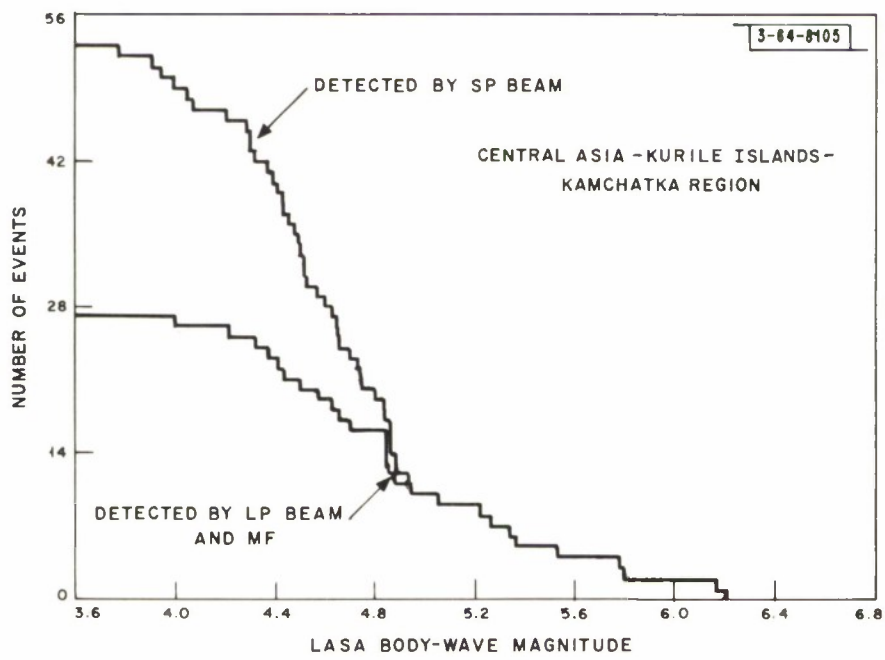
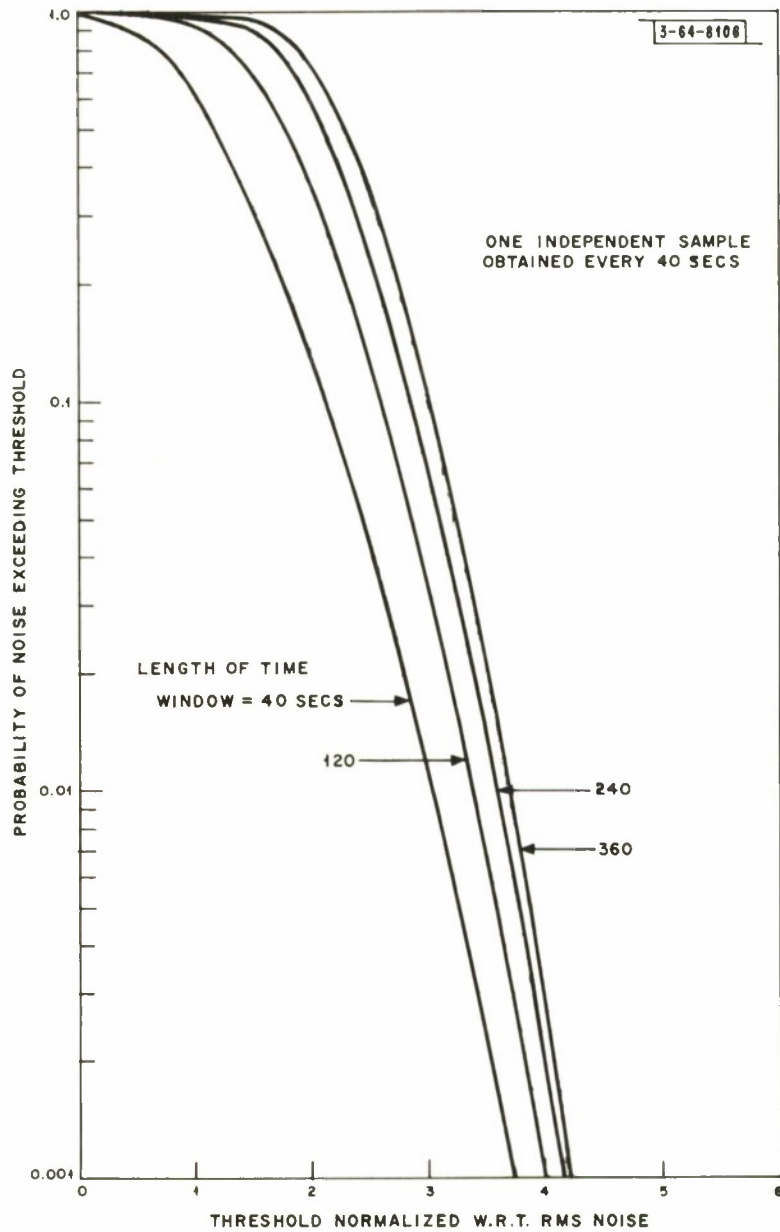
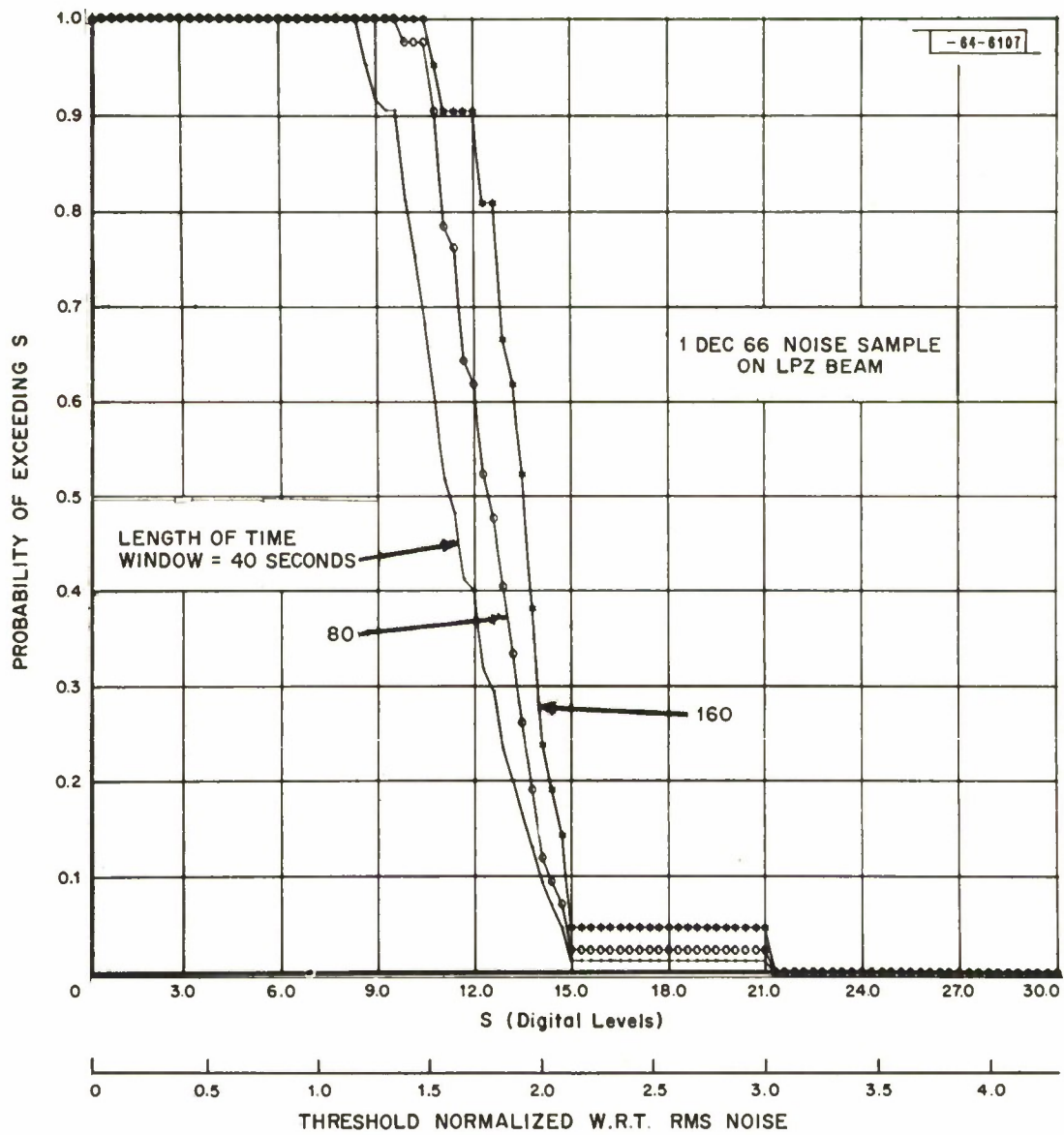


Fig. 22. Cumulative distribution of events detected in Central Asia-Kurile Islands-Kamchatka regions.



(a) Theoretical model.

Fig. 23. Probability of noise alone exceeding a given level vs threshold for various lengths of time window.



(b) Experimental results.

Fig. 23. Continued.

DOCUMENT CONTROL DATA - R&D

(Security classification of title, body of abstract and indexing annotation must be entered when the overall report is classified)

1. ORIGINATING ACTIVITY (Corporate author) Lincoln Laboratory, M. I. T.		2a. REPORT SECURITY CLASSIFICATION Unclassified	
		2b. GROUP None	
3. REPORT TITLE Long-Period Signal Processing Results for Large Aperture Seismic Array			
4. DESCRIPTIVE NOTES (Type of report and inclusive dates) Technical Note 1967-50			
5. AUTHOR(S) (Last name, first name, initial) Capon, Jack, Greenfield, Roy J. and Lacoss, Richard T.			
6. REPORT DATE 15 November 1967		7a. TOTAL NO. OF PAGES 82	7b. NO. OF REFS 15
8a. CONTRACT OR GRANT NO. AF 19 (628)-5167		9a. ORIGINATOR'S REPORT NUMBER(S) TN-1967-50	
b. PROJECT NO. ARPA Order 512		9b. OTHER REPORT NO(S) (Any other numbers that may be assigned this report) ESD-TR-67-564	
c.			
d.			
10. AVAILABILITY/LIMITATION NOTICES This document has been approved for public release and sale; its distribution is unlimited.			
11. SUPPLEMENTARY NOTES None		12. SPONSORING MILITARY ACTIVITY Advanced Research Projects Agency, Department of Defense	
13. ABSTRACT <p>The results of a series of off-line signal processing experiments are presented for long-period data obtained from the Large Aperture Seismic Array (LASA) located in eastern Montana. The signal-to-noise ratio gains obtained with maximum-likelihood processing, as well as other simpler forms of processing, are presented for body-wave as well as surface-wave phases. A discussion of the frequency-wavenumber characteristics of the noise which led to these results is also given. On the basis of these experiments several recommendations are made concerning optimum long-period array configurations and on-line or off-line processing methods.</p> <p>The usefulness of maximum-likelihood processing in suppressing an interfering teleseism is demonstrated. An experiment is given in which maximum-likelihood processing achieved about 20-db suppression of an interfering teleseism, while simpler forms of processing such as beamforming obtained about 11 db.</p> <p>The matched filtering of surface waves using chirp waveforms is also discussed. The most useful discriminant for distinguishing between natural seismic events and underground nuclear explosions, using both the long-period and short-period data, was found to be that based on the relationship between the surface-wave and body-wave magnitudes. Measurements of this discriminant made on events from four tectonic regions of the earth are presented. It is shown that 60, 100 percent detectability of surface waves for natural seismic events from the Central Asian-Kurile Islands-Kamchatka region occurs at about LASA body-wave magnitudes 4.5, 4.9, respectively.</p>			
14. KEY WORDS seismic array LASA signal processing			